

## Article

# Modeling of Floor Heave in Underground Roadways in Dry and Waterlogged Conditions

Piotr Małkowski <sup>1,\*</sup> , Łukasz Ostrowski <sup>1</sup> and Jerzy Stasica <sup>2</sup>

<sup>1</sup> Department of Geomechanics, Civil Engineering and Geotechnics, Faculty of Civil Engineering and Resource Management, AGH University of Science and Technology, 30-059 Krakow, Poland; lukost@agh.edu.pl

<sup>2</sup> Department of Mining Engineering and Occupational Safety, Faculty of Civil Engineering and Resource Management, AGH University of Science and Technology, 30-059 Krakow, Poland; stasica@agh.edu.pl

\* Correspondence: malkgeom@agh.edu.pl; Tel.: +48-604-055-842

**Abstract:** Floor heaving is a phenomenon that occurs in almost all mining roadways and tunnels. It can restrain the advance of the heading face or cause serious problems during roadway use. The highest levels of floor uplifting are observed in coal mines, which can reduce the output or even stop it altogether. The floor heaving intensity depends on the rock type, the stress in the rock mass, and rocks' mechanical properties. Floor deformation develops when the secondary state of stress is formed around the working, and it is much higher and more dynamic in the case of waterlogged rocks. The presence of water increases the floor's propensity to heave, especially clay rocks, such as claystones or mudstones, if they include water-absorbed minerals. In this paper, we present a new modeling methodology for roadway floor heave. The modeling covers a dry floor condition in which the parameters of the Hoek-Brown failure criterion are gradually lowered over time, and a waterlogged floor condition, in which the strength and strain parameters of the rocks are gradually reduced in line with their progressive saturation. In the second case, the claystone floor's geomechanical parameters were investigated, and the rocks were subjected to water for up to 24 h. The results of the numerical simulation were compared with the in situ measurements of convergence and floor heave in the same coal mines from which the rock samples were collected. The consistency between the numerical simulations and the underground measurements reached 90–99%.

**Keywords:** floor heave modeling; underground roadway; waterlogged rock; floor uplift over time; floor damaged rock; floor heaving phenomena



**Citation:** Małkowski, P.; Ostrowski, Ł.; Stasica, J. Modeling of Floor Heave in Underground Roadways in Dry and Waterlogged Conditions. *Energies* **2022**, *15*, 4340. <https://doi.org/10.3390/en15124340>

Academic Editor: Manoj Khandelwal

Received: 25 April 2022

Accepted: 9 June 2022

Published: 14 June 2022

**Publisher's Note:** MDPI stays neutral with regard to jurisdictional claims in published maps and institutional affiliations.



**Copyright:** © 2022 by the authors. Licensee MDPI, Basel, Switzerland. This article is an open access article distributed under the terms and conditions of the Creative Commons Attribution (CC BY) license (<https://creativecommons.org/licenses/by/4.0/>).

## 1. Phenomenon of Floor Heave

The heaving of the floors of underground openings is a common occurrence in almost all mining and tunneling projects. Considering that the total length of roadways excavated in the world each year is in the range of thousands of kilometers, the problem of floor heave is extensive. Guo [1] notes that in China only, the total length of maintained roadways each year in coal mines is at least 8000 km. In each coal mine in Poland, 10 to 20 km of roadways are excavated every year, and there are no less than 100–150 km of roadways where floor heaving occurs.

Floor heaving varies in magnitude and characteristics. Within weak, easily breakable rock masses, it is continuous, and appears both at the sidewalls and in the middle of the floor, where it is usually slightly higher (Figure 1a). At the same time, the roofs of roadways are damaged. In these conditions, the heave usually reaches several tens of centimeters [2–5]; it reaches dozens to tens of centimeters even if floor reinforcement is installed [1,2,4,6,7]. In the case of strong rock mass, the heave manifests itself as a crack in the underlying rock bed due to its buckling, and usually produces the asymmetric uplift of rock slabs (Figure 1b). Both cases cause transport obstruction and technical problems for roadway users.

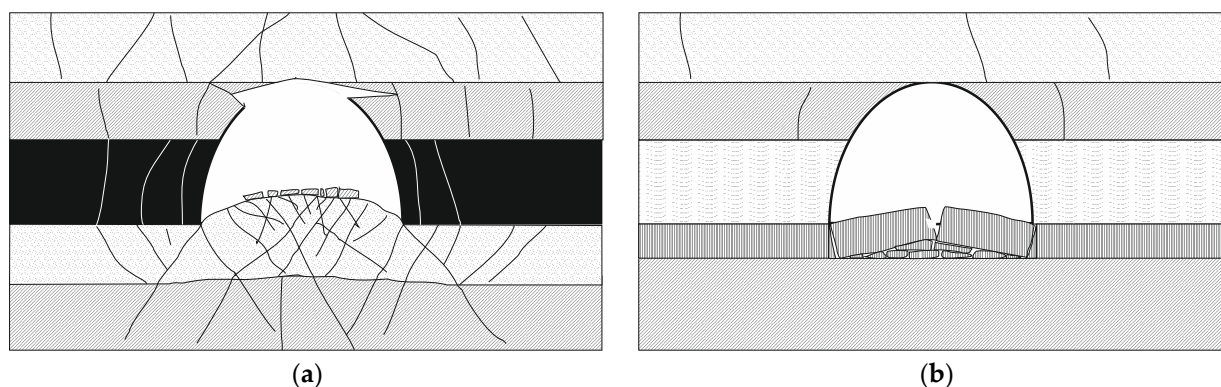


**Figure 1.** Heave of floor rocks. (a) Weak rocks, (b) strong rocks.

It can be concluded that the main cause of floor heaving is either the stress exceeding the strength limit of the rock or, in weak and fractured rock masses, gradual destruction towards post-failure rock conditions. In this process, the rock-mass strength parameters and the post-failure parameters change gradually. Wang [8] reported interesting research on physical models of floor heave.

The gradual transition of the floor's rock bed from its original state into a post-failure condition is comprehensively described by Li [9]. He pointed out that apart from the rock properties, the key factors in floor heaving are the changes in the stress conditions caused by roof-rock failure. The additional load from rock beds breaking in the roof results in increased stress in the sidewalls, which affects the underlying rock in the floor. Hairline fissures appear first, which then open up, propagate and connect to form a fractured zone (Figure 2), which increases in volume. The damage in laminated sedimentary rock usually starts along laminae (Figure 2a) and the final apertures are the biggest there (Figure 2c). The rock bed, which initially works as a continuous beam, loses its integrity, and gradually heaves. Finely layered rock beds are particularly prone to heaving. The magnitude and rate of heaving depend on the existing stress conditions and the vertical–horizontal-stress ratio [1,6]. The asymmetry of the floor heave is strongly related to the dip in the rock beds [10].

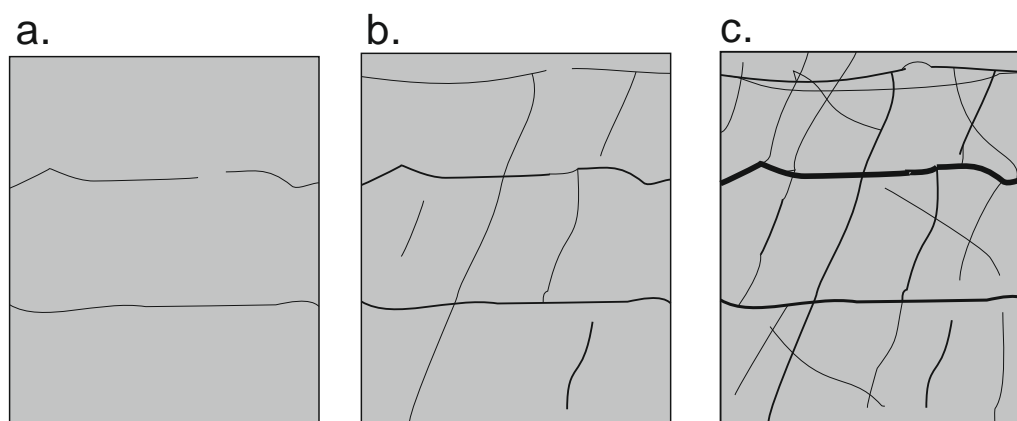


**Figure 2.** Propagation of fractures along with stress increase (a) fracture initiation, (b) fracture development, (c) fracture expansion.

The currently used analytical solutions [7,11,12] clearly depict the mechanism of the heave phenomenon, yet they fail in terms of quantities. Numerical methods are the best ways to model the magnitudes and spatial distribution of deformations. They can be applied to any mining conditions, such as the determination of the heave and the deformation of roadways [10,13–15], the design of roadways to be maintained along the goaves [3], the determination of the exploitation front's impact on the floor heave in the gate entries [2–4,8,16], including the use of backfill [17], and trials on new methods of

floor-heave prevention [2,6,7,12,18–22]. In the aforementioned works, the authors obtained broad ranges of values of floor heave, depending on the assumed mining and geological conditions, the geomechanical rock parameters, the depth of the roadway, its dimensions, and the assumed stress conditions. Next, the calculation results were compared with the in situ measurements in the underground roadways. The comparison shows that at a depth of 280 m in shaley rocks, the estimated floor heave was 710 mm, compared the 735 mm measured in the roadway [4]; at a depth of 530 m in clay rocks, the heave was 316 mm compared with 462 mm for the roadway [2]; at 580 m in sandy mudstone, it was approximately 550 mm, compared with 590 mm [3]; and at 1030 m in weak mudstone, it was approximately 270 mm, compared with 400 mm [22]. Generally, all the authors used elasto-plastic numerical models in their research, with the exception of Guo and Lu [22], who used a creep visco-elastic model.

It needs to be highlighted that in some of the reports, the authors considered in the models the rock bolts or shotcrete in the floor, which limited the heave and, therefore, did not show its full scale. The reports also show that there is no universal modeling methodology, and that every case needs to be resolved separately.

The methods used for floor heave determination also include index methods [23–25]. These allow the estimation of the scale of the heave hazard and the indication of its key factors, yet they do not allow precise heave prediction.

## 2. Effect of the Presence of Water on the Floor Heave

The presence of water increases floors' propensity to heave. Pimentel [26] points out that in such conditions, one of the key factors is the mineralogical composition of rocks (e.g., the amount of swelling and non-swelling clay minerals, anhydrite, or pyrite), and the chemical contamination of water (e.g., sulphates, or other salts). The strongest factor is the content of swelling clay minerals, which weaken the rock, and decrease the strength parameters by up to 70% [27]. However, based on their experience, the authors of index-based methods assign different weights to the presence of water as a contributor to floor heaving. The authors of [24] concluded that for the gate entries, out of seven distinguished factors, the water pressure in the rock mass was ranked sixth. Its weight was assigned as three times lower than the depth of the roadway and the cohesion of the rocks, six times lower than the distance to the exploitation front, and equal to the rock beds' inclination. Aghababaei [23] and Mo [25] do not consider water at all as a key factor in floor heave, even though they do consider the underlying rocks' Young's modulus, which varies significantly, depending on moisture content.

One of the infrequent research projects that considered the impact of the presence of water on the rock mass around the roadway in terms of floor heave was presented by Tang and Tang [28]. The authors proposed a numerical model based on humidity diffusion to simulate floor heaving processes. The authors assumed that the major mechanical factors necessary for the modeling of the deformation of water-saturated rocks, i.e., compressive strength, Young's modulus, and Poisson's coefficient, vary, depending on the degree of water content. They also assumed that the observed deformation is a sum of elastic and humid strain. Further, the flow equation was used to determine the diffusion of moisture versus time in the rock mass around the roadway, which in turn allowed the demonstration of the floor heave together with the deepening water-permeated zone in the rock mass (Figure 3).

Computerized simulation, performed for different values of horizontal stress, allows the determination of the longest-possible duration of the swelling and heaving of floor rocks, and the maximum heave value. After 70 days, in the rocks with initial Young's modulus 1 GPa and relative moisture content 20%, the heave may reach a maximum of approximately 680 mm. However, the most significant observation is not the quantitative aspect of the modeling of the phenomenon, but the confirmation of the process of rock degradation by water permeating the rock mass, which lasts for a determinable time.

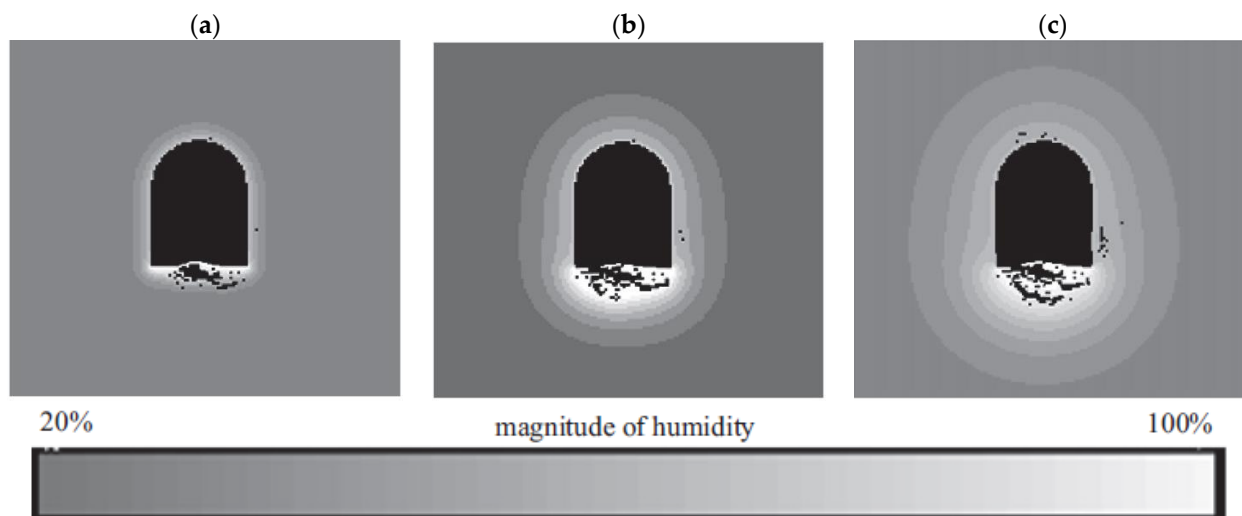


**Figure 3.** Moisture diffusion processes during floor heave associated with failure evolution (a) after 10 days, (b) after 30 days, and (c) after 70 days [28].

Li [9] writes that the records of water inrush events in mining fields show large subsidence of the roadway floor occurring just before the water inrush. This is explained by fractures in the floor rapidly developing downward and interconnecting, thereby radically increasing the permeability, which causes the water influx in the longwall face, roadways, and goaves. The destruction of the rock mass around a roadway is strongly related to its depth, which causes high vertical stress and the concentration of vertical stress  $\sigma_z$  in the sidewalls, as well as horizontal stress  $\sigma_x$  concentrations on the floor. The destruction process intensifies over time (Figure 4).

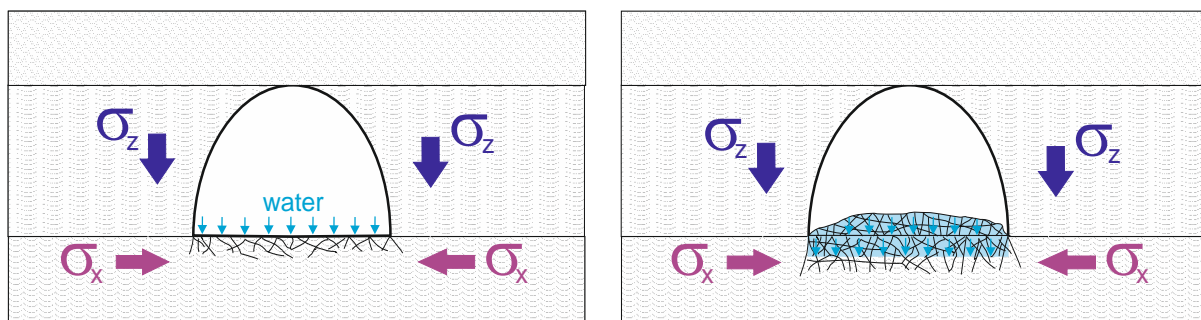


**Figure 4.** Gradual permeation of water through fractured zone into the rock mass on the floor.

The aforementioned observations clearly indicate that the data that are critical to the modeling of waterlogged floors are the values of the geomechanical parameters of saturated rocks beneath roadway floors. The strength of these rocks degrades gradually, together with water permeating through the developing fractures. Therefore, in the model, the strength and deformability parameters cannot be assumed to be constant; they must be progressively reduced over time. To achieve this, the samples collected from beneath the floor that are unaffected by water rocks must be tested in the laboratory with various moisture contents. To this end, typically, samples in the laboratory are submerged in water for certain periods, e.g., 3, 6, 12, and 24 h. The laboratory periods correspond to much longer times of rock exposure to water in roadways because in real conditions, the rock is not submerged—it is exposed to air humidity and seepages. Usually, a 24-h period of submergence in water is long enough for complete saturation and reaction with water, even for clay rocks [29]. In certain cases, this period may be shorter [27].

In this paper, we present a new modeling methodology for roadway-floor heave. The modeling is based on dry-floor conditions, in which the parameters of the Hoek–Brown failure criterion are gradually lowered over time, and waterlogged-floor conditions, in which the strength and strain parameters of rocks are gradually reduced in line with their progressive saturation.

In the first case, it was necessary to determine the variance functions of the  $m_b$  and  $s$  parameters for each type of rock by in situ measurements, which were carried out on Carboniferous rocks in two coal mines. In the second case, laboratory deformation and strength-parameter tests were performed on floor rocks subjected to water to various degrees. Further, the obtained results were used in the model when gradually lowering the values of the geomechanical parameters. Furthermore, in this case, the results of the numerical simulation were compared with the in situ measurements of convergence and floor heave in the same coal mines from which the rock samples were collected. For the verification of the modeling, two roadways with changing conditions (with sections of dry rock and waterlogged rock) were selected.

### 3. Numerical Modeling of Roadway Floor Deformations

#### 3.1. Assumptions of the Model

The numerical simulations of two-dimensional deformation of roadway floor heave were performed using the Phase 2 program, which is based on the finite elements method. In both cases, the rock-mass model covered a two-dimensional rectangular section with a size of 60 by 60 m. Zero vertical and horizontal displacement along the boundaries of the section was assumed in the model. The modeled roadways' perpendicular sections were arch-shaped. In both cases, the yielding standing support was input into the models; however, due to its yield property, it did not affect the deformation of the contour of the roadway.

In the numerical simulations, the Hoek–Brown failure criterion was used, as expressed by the following equation:

$$\sigma'_1 = \sigma'_3 + \sigma_{ci} \left( m_b \frac{\sigma'_3}{\sigma_{ci}} + s \right)^{a_s} \quad (1)$$

where:

$\sigma'_1, \sigma'_3$ —maximum and minimum effective stress at failure;

$\sigma_{ci}$ —uniaxial compressive strength of intact rock sample;

$m_b$ —Hoek–Brown constant for rock mass;

$s, a_s$ —constants that depend upon the rock mass characteristics.

The parameters characterizing the rock mass in the Hoek–Brown failure criterion equation (1) are the terms  $m_b$  (2) and  $s$  (3), which depend on the rock-mass quality index GSI (or  $GSI = RMR - 5$  [30]). For the determination of the  $m_b$  and  $s$  parameters, the variable  $D$  was assumed to be 0, which corresponds to Hoek's classification category: "mechanical excavation in poor quality rock masses (no blasting) resulting in minimal disturbance to the surrounding rock mass".

$$m_b = m_i \exp\left(\frac{GSI - 100}{28 - 14D}\right) \quad (2)$$

$$s = \exp\left(\frac{GSI - 100}{9 - 3D}\right) \quad (3)$$

where:

$m_i$ —Hoek–Brown constant for rock mass;

$GSI$ —Geological Strength Index;

$D$ —rock mass disturbance factor;

Furthermore, the GSI value used in Equations (2) and (3) was calculated from the RMR index derived from the laboratory strength tests, the examination of the drill cores, and the site inspection in the roadway. Thanks to the aforementioned research, the values of the

six required parameters of the RMR system were determined [31]: strength of intact rock, RQD, spacing of discontinuities, condition of discontinuities, groundwater conditions, and effect of discontinuity strike and dip orientation on drivage. The RMR represented a zone up to 10 m above the roof and 3 m beneath the floor of the roadway. The results of the geomechanical investigation in the mines' geological documentation were also used for the determination of the RMR.

The triaxial compression test results were not available. Therefore, the determination of the material constant  $m_i$  was based on the equation developed by Davarpanaha [32] for sedimentary rocks (Equation (4)), where  $\sigma_{ci}$  is the uniaxial compressive strength and  $\sigma_t$  is the tensile strength:

$$m_i = e \left[ 1.3 \left( \frac{\sigma_{ci} - 2.5\sigma_t}{\sigma_t} \right) \right]^{0.26} \quad (4)$$

For both variants of the modeling, i.e., for the floor rocks not exposed to the water, only to the time factor, and for the waterlogged floor rocks, the calibration of the models was performed based on the in situ heave and convergence measurements from roadways D-2 and F-33 [32]. The measurements were carried out over 703 and 233 days, which was sufficiently long for the determination of the rock-mass property changes for modeling purposes and for the verification of the numerical modeling.

### 3.2. Models and Parameters of Rock Beds

#### 3.2.1. Roadway D-2

Roadway D-2 was 6.5 m wide at floor level and 4.225 m high. It was driven at an average depth of 1000 m in the "Zofiowka" coal mine, along the strike. The dip was ca. 6°. The geomechanical parameters assumed for the roadway D-2 model are shown in Table 1, and the model section is shown in Figure 5.

**Table 1.** Geomechanical parameters of rocks around roadway D-2.

Strata	Rock Bed	Bed Thickness $h_i$ (m)	Bulk Weight $\gamma_i$ (kN/m <sup>3</sup> )	Compressive Strength $\sigma_{ci}$ (MPa)	Young Modulus $E_i$ (GPa)	Poisson Ratio $\nu_i$ (-)
Roof	Sandstone	2.5	25.32	75.4	9.02	0.29
	Claystone	2.0	24.19	42.5	4.89	0.32
	Mudstone	2.0	25.27	46.9	7.12	0.30
	Sandstone	3.8	24.87	64.1	8.21	0.28
	Mudstone	2.7	25.01	41.2	6.98	0.32
	Claystone	1.0	24.14	29.8	4.13	0.27
	Coal seam 411/3	0.8	13.02	10.2	1.57	0.30
	Claystone	1.0	24.74	32.5	3.26	0.32
	Sandstone	8.5	25.32	85.8	11.78	0.29
	Claystone	1.4	24.47	45.4	4.48	0.23
Sidewall	Coal seam 412	4.6	12.13	21.4	2.12	0.31
Floor	Claystone	3.5	25.17	56.1	5.16	0.21
	Mudstone	4.8	26.33	61.3	8.19	0.31
	Claystone	2.5	25.02	48.2	4.21	0.31
	Coal seam 413/2	2.6	12.50	8.1	2.02	0.30
	Claystone	0.5	26.73	28.2	2.19	0.32
	Mudstone	8.0	25.46	71.2	8.45	0.27
	Claystone	0.4	24.78	25.6	2.09	0.35
	Coal seam 415 Mudstone	0.6 6.8	12.72 26.02	11.1 58.9	1.98 6.42	0.30 0.31

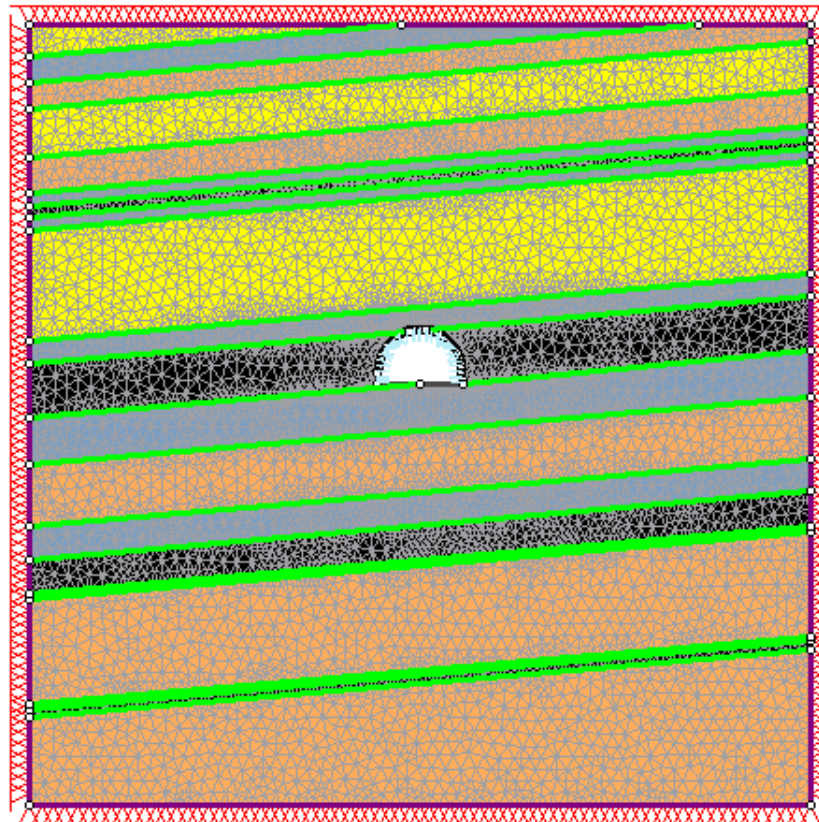


**Figure 5.** Numerical model section of the roadway D-2.

Table 2 presents the RMR index, compressive and tensile strength ( $\sigma_c$  and  $\sigma_t$ ),  $m_i$  constant (both the value from the Formula (4) and the value assumed for the model), and initial values of  $m_b$  and  $s$  for the rock types around the roadway. Due to the moisture content in the shales of several percentage points, the calculated value of parameter  $m_i$  was slightly reduced for use in the model. The rock-mass quality was determined for the rock beds closest to the roadway D-2 contour; therefore, the values of the  $m_i$ ,  $m_b$ , and  $s$  parameters were assumed for each rock type rather than for the position against the contour, whereas the strength and deformability parameters differed depending on the position, as shown in Table 1.

**Table 2.** Parameters of rocks from around roadway D-2.

Rock Type	$\sigma_c$ (MPa)	$\sigma_t$ (MPa)	RMR	Rock Mass Class	$m_i$ calc	$m_i$ model	$m_b$	$s$
Claystone	45.38	4.51	44	III	9.02	8	1.083	0.0020
Mudstone	43.89	4.22	49	III	9.25	8	1.218	0.0035
Sandstone	69.65	5.01	54	III	11.56	12	2.301	0.0060
Coal	21.42	0.98	36	IV	16.59	17	1.729	0.0008

### 3.2.2. Roadway F-33

The F-33 roadway was 6.1 m wide at the floor and 4.225 m high. Its depth from the surface was 923 m. It was driven in the “Borynia” coal mine, along the strike. The dip was ca. 3°. The geomechanical parameters of the rocks around the F-33 roadway assumed for its numerical model are presented in Table 3, and the section of the model is shown in Figure 6.

**Table 3.** Geomechanical parameters of rocks around roadway F-33.

Strata	Rock Bed	Bed Thickness $h_i$ (m)	Bulk Weight $\gamma_i$ (kN/m <sup>3</sup> )	Compressive Strength $\sigma_{ci}$ (MPa)	Young Modulus $E_i$ (GPa)	Poisson Ratio $\nu_i$ (-)
Roof	Claystone	3.5	25.483	45.81	4.583	0.285
	Coal seam 401	2.5	12.413	17.13	1.135	0.300
	Clayey shale	6.6	26.242	67.71	7.421	0.305
	Mudstone	1.7	26.129	102.73	9.506	0.270
	Claystone	4.3	25.248	62.63	5.687	0.295
	Mudstone	8.4	26.008	74.39	8.423	0.270
	Claystone	3.0	25.352	43.72	4.707	0.215
Sidewall	Coal seam 403	2.0	12.066	15.89	1.018	0.310
Floor	Claystone	15.3	30.552	59.64	5.575	0.200
	Mudstone	1.4	25.937	68.45	5.126	0.280
	Claystone	11.3	25.809	54.48	4.875	0.255

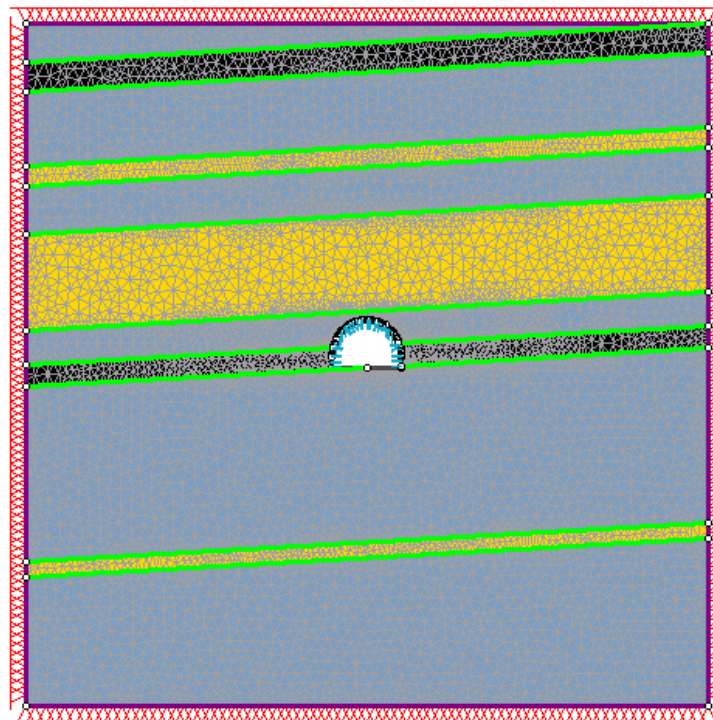
**Figure 6.** Numerical model section of roadway F-33.

Table 4 presents the RMR index, compressive and tensile strength ( $\sigma_c$  and  $\sigma_t$ ),  $m_i$  constant (both the value from Formula (4) and the value assumed for the model), and the initial values of  $m_b$  and  $s$  for the rock types around the roadway F-33. The rock-mass quality was determined only for the two rock beds in the roof of the roadway F-33 and for the coal seam; therefore, the values of the  $m_i$ ,  $m_b$ , and  $s$  parameters were assumed for each rock type rather than for the position against the roadway contour, whereas the strength and deformability parameters differed, depending on the position, as shown in Table 3.

**Table 4.** Parameters of rocks around roadway F-33.

Rock Type	$\sigma_c$ (MPa)	$\sigma_t$ (MPa)	RMR	Rock Mass Class	$m_{i\text{ calc}}$	$m_{i\text{ model}}$	$m_b$	$s$
Claystone	43.72	4.72	42	III	8.47	8	1.083	0.0020
Mudstone	73.49	6.84	43	III	9.49	9	1.218	0.0035
Coal	20.89	1.02	36	IV	15.73	16	1.729	0.0008

### 3.3. Roadway Floor Heave over Time

In the case of floor heave, when there are no factors that strongly affect the initial physical properties of the rocks, the post-excitation stress distribution develops over a long time. Cracks form in the nearest surroundings of the roadway, and the rock mass weakens. Therefore, for the modeling of this process, the values of the parameters of the Hoek–Brown criterion of the rocks around the roadway have to be lowered [33]. As demonstrated by Wei [34], the parameter  $m_b$  is changed by the critical crack, initial fractures, and confining pressure, while  $s$ , which expresses the rock integrity, is changed by the current principal stress  $\sigma_1$ .

Prior to the determination of the variance function of the changes in the values of these parameters, the convergence of the roadway has to be monitored over a certain time. The measurement results can further be used for the prediction of the rock-mass parameter reduction and, subsequently, for the floor-heave prediction in other sections of the roadway, where the surrounding rocks are of the same type. Therefore, the in situ convergence measurements in the roadway should commence as early as possible. In the numerical model, the values of the  $m_b$  and  $s$  parameters of the surrounding rocks were adjusted to achieve consistency between the model results and the convergence measurements at the monitoring station at the roadway. For practicality, it was assumed that the consistency between the generated and the measured results was satisfactory if the difference between them did not exceed 20%. The in situ records show that the convergence of the roadway can be described as a power function (Figure 7 [5]). Therefore, it can be inferred that the trendlines of the changes in the rock mass parameters must be of the opposite character, i.e., logarithmic.

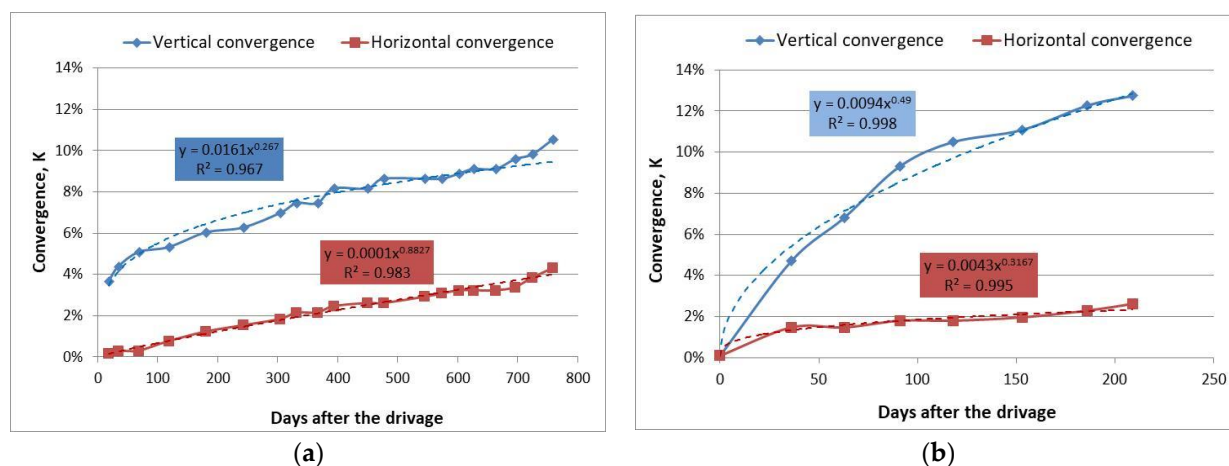


**Figure 7.** Development of convergence of roadways—underground measurements. (a) The 595th meter of roadway D-2. (b) The 405th meter of roadway F-33.

#### 3.3.1. Roadway D-2

Convergence measurements and numerical modeling were carried out for the monitoring station at the 595th meter of roadway D-2. Since the convergence-monitoring station was installed 118 days after excavation of the roadway, the determination of the Hoek–Brown parameters began after a significant delay.

In the first step of the numerical modeling, the convergence was calculated with the assumption of elasto-plastic rock mass with reinforcement; therefore the post-failure parameters of the rock mass were not reduced (Figure 8). The simulated convergence of the roadway, rounded to the nearest whole number, was as follows:

- Roof sagging—2 cm;
- Maximum floor heave—9 cm;
- Average floor heave—6 cm;
- Convergence of sidewalls—8 cm.

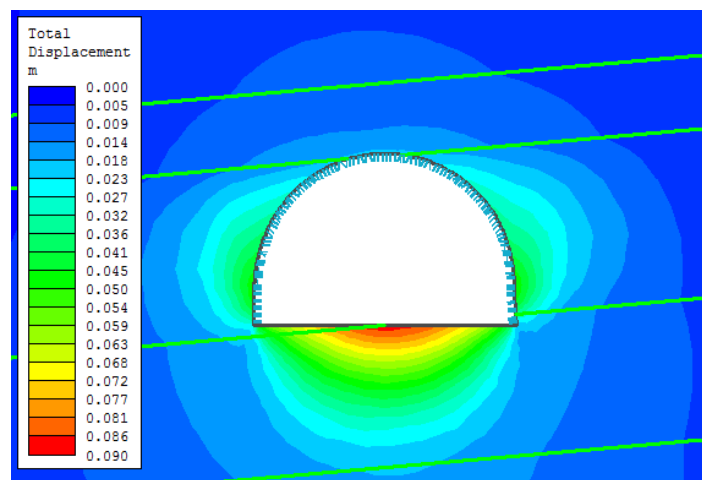


**Figure 8.** Results of numerical modeling of rock deformation around roadway D-2 for elasto-plastic rock mass with reinforcement.

The roadway deformation chart obtained from the model is shown in Figure 8. The charts for the deformation around the roadway D-2 calculated after 180, 360, 573, and 724 days after the excavation are shown in Figure 9. The comparison of the numerical simulation results with the in situ measurements is given in Figure 10. The chart lines of the numerical results and measurements of the convergence and floor uplift differ from each other at some points by a maximum of 20%. This proves the high consistency between the measured and the modeled deformation values.

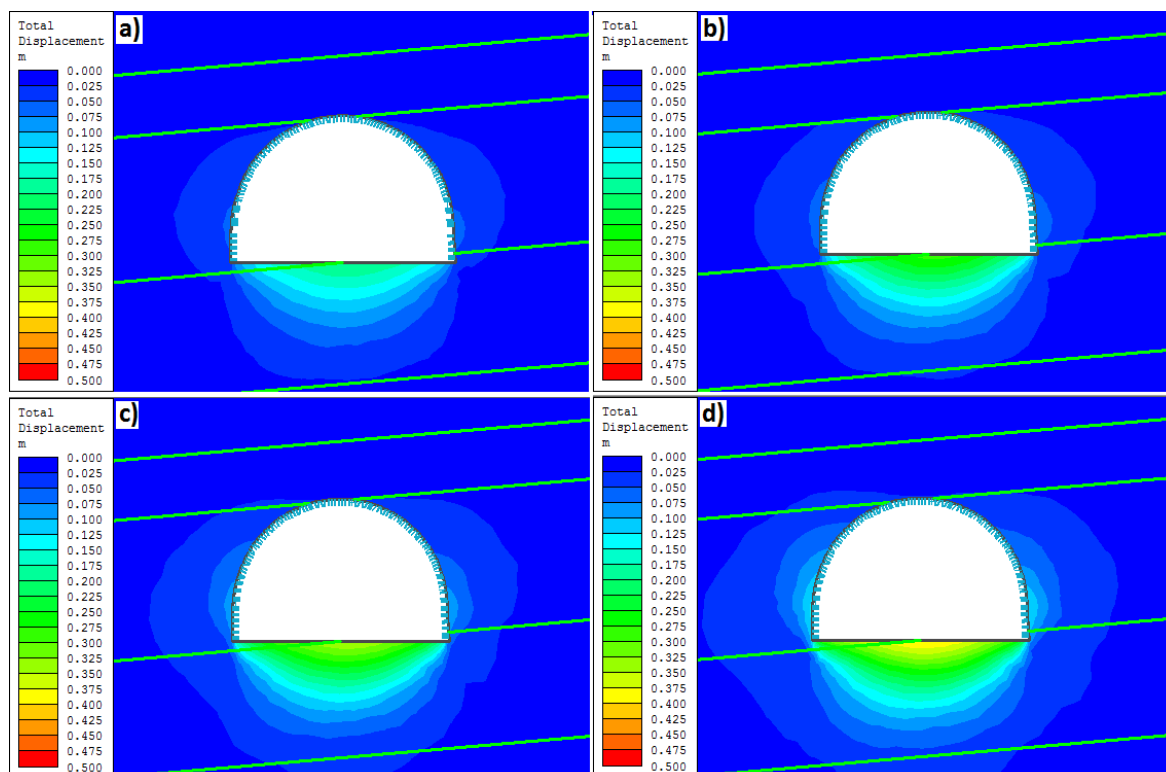


**Figure 9.** Charts of rock mass deformation around roadway D-2—chainage 595 m. (a) Deformation corresponding to measurements 180 days after roadway excavation. (b) Deformation corresponding to measurements after 366 days after roadway excavation. (c) Deformation corresponding to measurements after 573 days after roadway excavation. (d) Deformation corresponding to measurements after 724 days after roadway excavation.

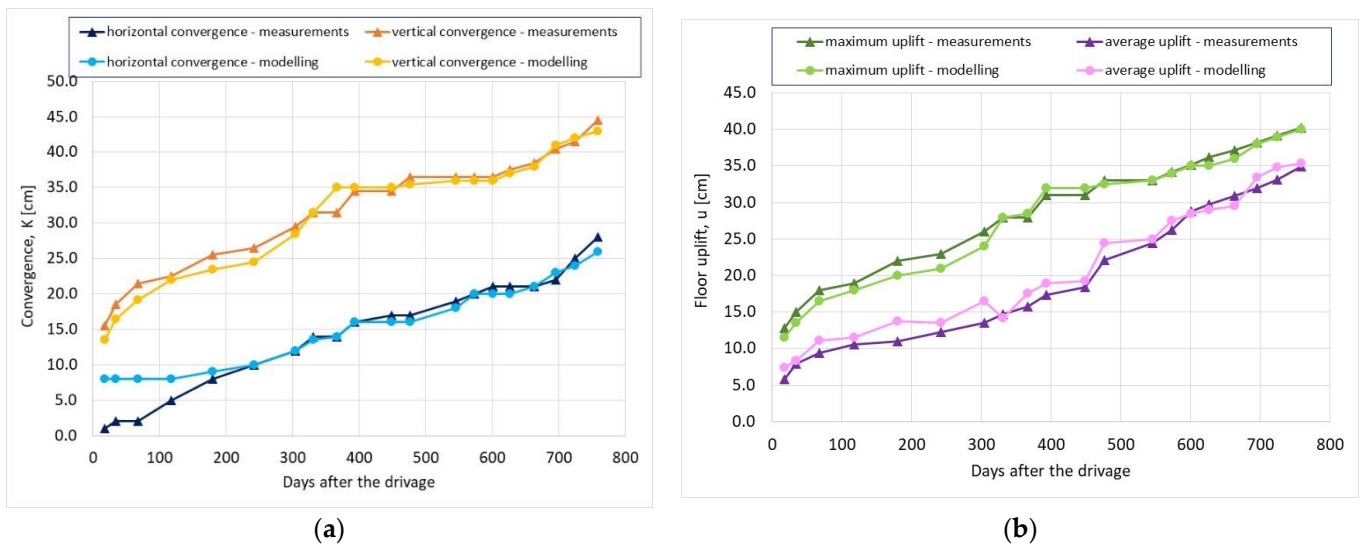


**Figure 10.** The consistency between numerical modeling and underground measurements of roadway D-2 deformation—chainage 595 m. (a) Convergence. (b) Floor uplift.

The graphs in Figures 11 and 12 illustrate the changes in the  $m_b$  and  $s$  parameters over the period used in the model. The numerical simulation shows that the  $m_b$  parameter of claystone decreases from the initial value 0.921 (18 days after the excavation of the roadway) down to 0.421 (758 days after the excavation), which is a 55% drop at a rate of 0.0007/day. In the same period, the parameter  $s$  shows an increase of over fivefold. A similar trend in the changes in the post-failure parameters can be observed for mudstone, for which the  $m_b$  and  $s$  values were 1.192 and 0.0033, respectively, 18 days after excavation, which represents a 55% drop in the  $m_b$  parameter (at a rate of 0.0008/day), and an 85% drop in the parameter  $s$ .

The Hoek–Brown parameters  $m_b$  and  $s$  of sandstone around the D-2 roadway decreased over 758 days from the roadway excavation, from 2.280 and 0.006 to 1.125 and 0.0006, respectively, which represents a 52% drop in the  $m_b$  value at a rate of 0.0016/day, and an 82% drop in the  $s$  value. For coal, the numerical simulation shows a 53% drop in the  $m_b$  value over the time from the excavation of the roadway (at a rate of 0.0013/day), and a 75% drop in the  $s$  value.

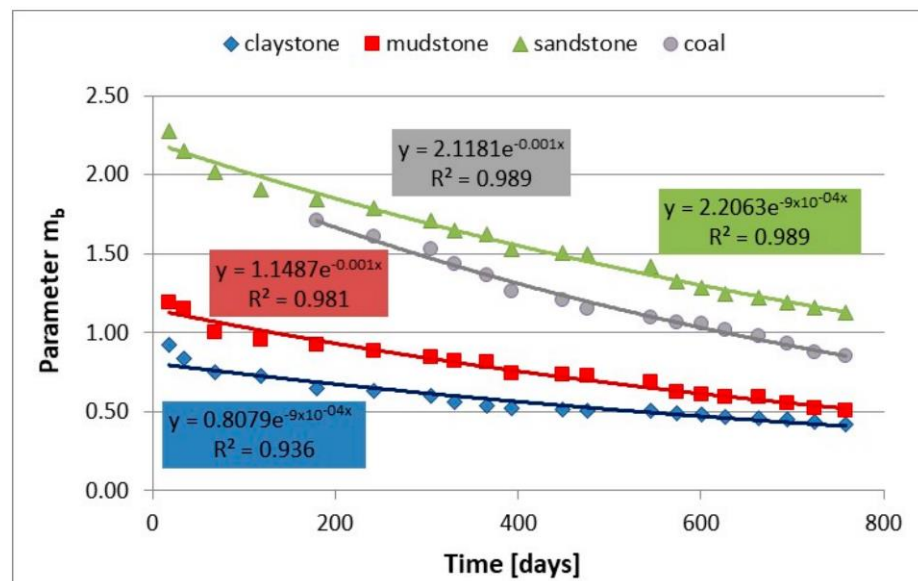


**Figure 11.** Changes in Hoek–Brown parameter  $m_b$  for rocks around roadway D-2, chainage 595 m.

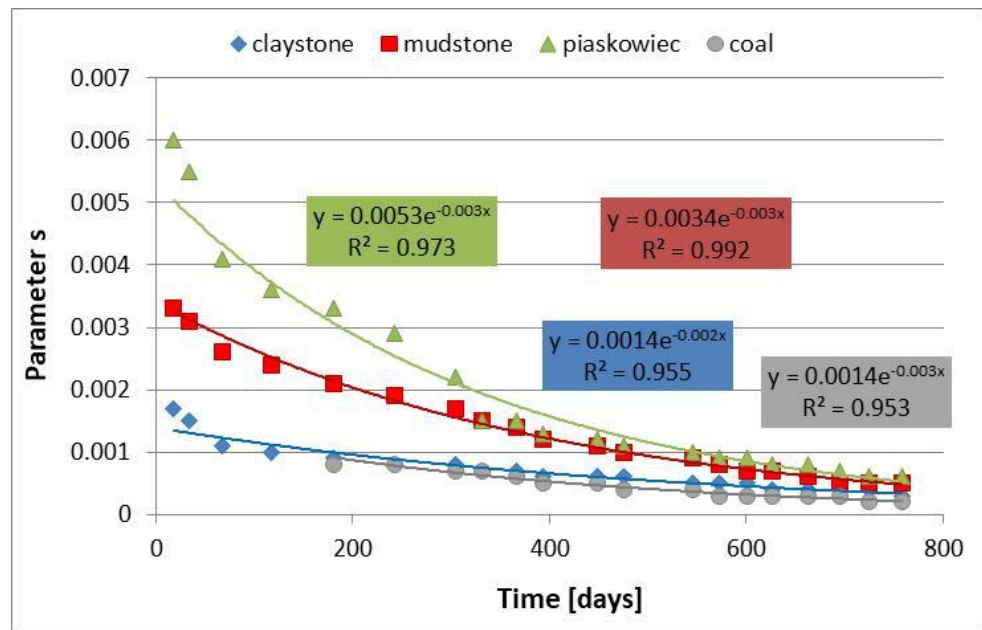


Figure 12. Changes in Hoek–Brown parameter  $s$  for rocks around roadway D-2, chainage 595 m.

As expected, the trendlines of the changes in the  $m_b$  and  $s$  parameters versus time since excavation are exponential functions, for which the coefficient of determination reaches high values within the 0.95–0.99 range. The trendlines and their corresponding equations are shown in Figures 11 and 12.

Changes in the RMR index with the reduction in the  $m_b$  and  $s$  values were also analyzed based on the performed numerical simulations. Together with rock-mass weakening, the changes in  $m_b$  and  $s$  values should also reflect the rock-mass quality reduction. However, the analysis shows that for the determined trendline functions of the reduction in the parameters of the Hoek–Brown criterion, there is no strong consistency with RMR changes (Figure 13).

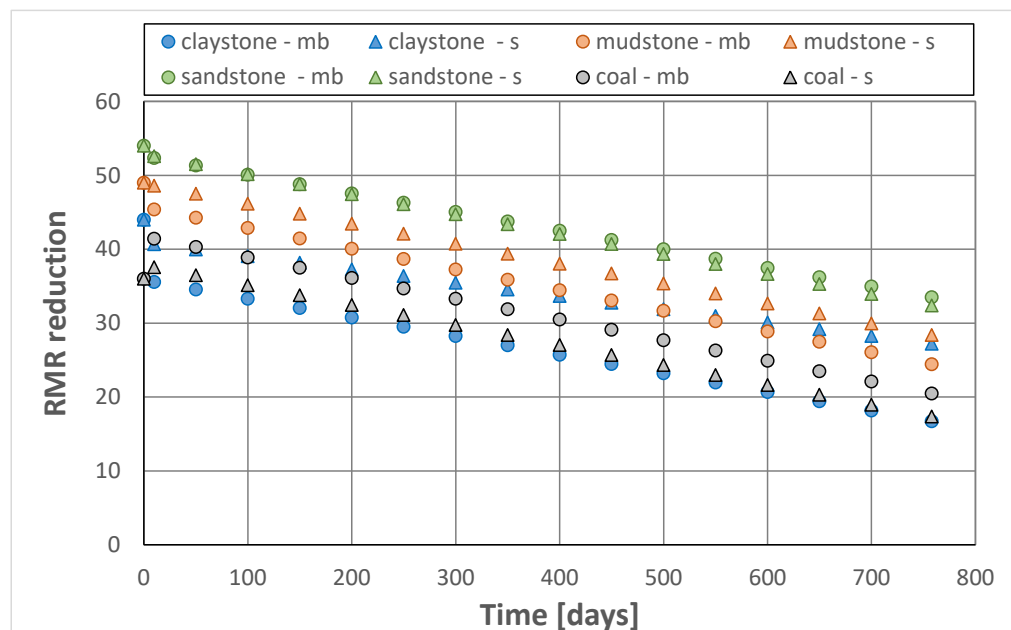


Figure 13. RMR decrease corresponding to  $m_b$  and  $s$  decrease versus time—rocks around roadway D-2.

In the case of sandstone, this inconsistency is negligible because, 758 days after the roadway excavation, it is as small as 3%. The inconsistency is still acceptable in the case of coal and mudstone, where it amounts to 13% and 16%, respectively; however, in the case of claystone, it reaches 64%, which indicates the inaccurate simulation of the  $m_b$  and  $s$  values. In addition, in the case of coal, there is a slight increase in the RMR index with respect to its initial value when applying the determined trend functions of the  $m_b$  and  $s$  parameters. Therefore, for a more precise evaluation of rock-mass quality reduction, there is a need for better calibration of the trend line functions of the changes in the H–B criterion parameters.

### 3.3.2. Roadway F-33

The numerical simulation of the convergence of the roadway F-33 was performed for the location of the convergence-monitoring station at 405th meter of the roadway.

The width of the roadway at the floor level was 6.1 m and its height was 4.225 m. As in the case of roadway D-2, the simulation was performed for elasto-plastic rock mass with reinforcement.

For these settings, the obtained deformation values were relatively low (Figure 14):

- Roof sagging—2 cm;
- Maximum floor heave—9 cm;
- Average floor heave—7 cm;
- Convergence of sidewalls—12 cm.

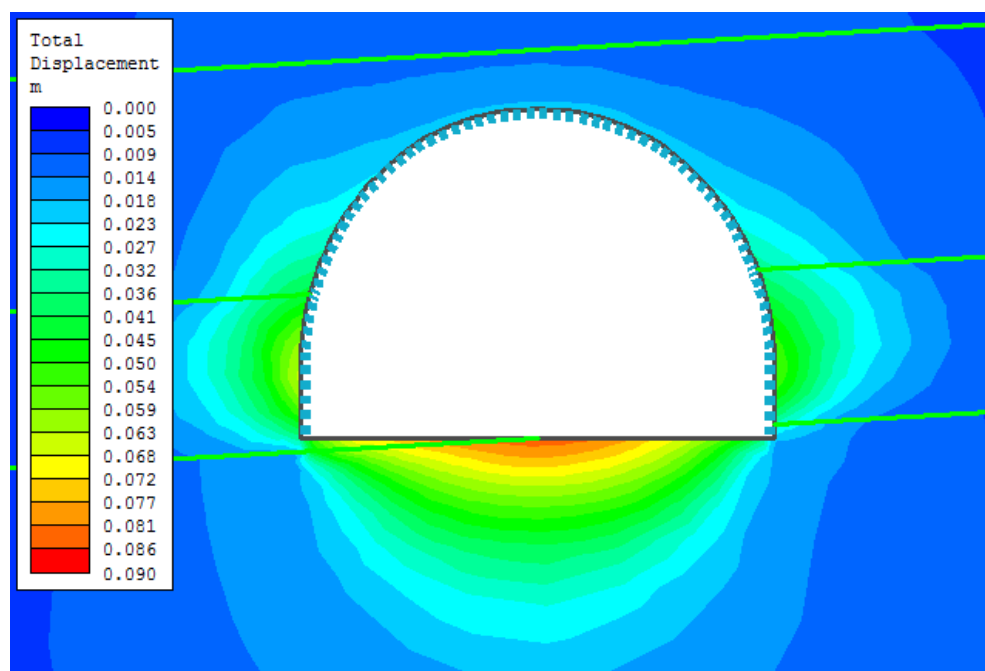


**Figure 14.** Initial convergence results for roadway F-33.

In the next step, by changing the post-failure parameters of the rocks with the time since excavation of the roadway, the values of deformations of the roadway contour, including the floor heave, were determined (Figure 15).

The results of the numerical simulation and the in situ measurements are juxtaposed in Figure 16. Differences between these measurements of more than 20% occur only in the case of the calculated change of the width of the roadway in the early stages of the model (up to 116 days after the excavation), and are in the range of 1.3–3.0 cm. Even though they are up to 25% of the measured convergence, these values are insignificant compared to the entire width of the roadway, 6.1 m.

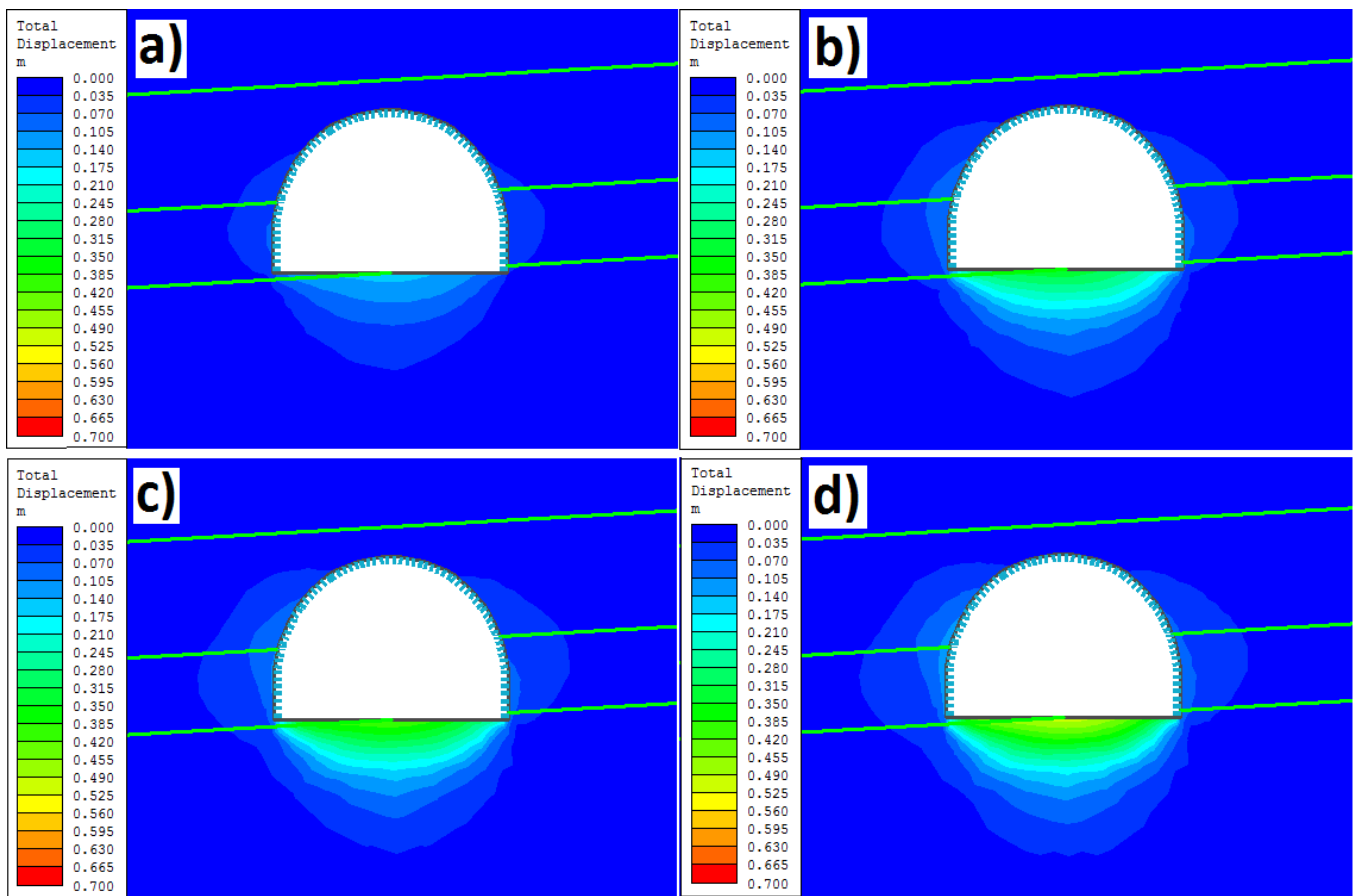


**Figure 15.** Charts of rock mass deformation around roadway F-33—chainage 405 m. (a) Deformation corresponding to measurements 36 days after roadway excavation. (b) Deformation corresponding to measurements 91 days after roadway excavation. (c) Deformation corresponding to measurements 153 days after roadway excavation. (d) Deformation corresponding to measurements 209 days after roadway excavation.

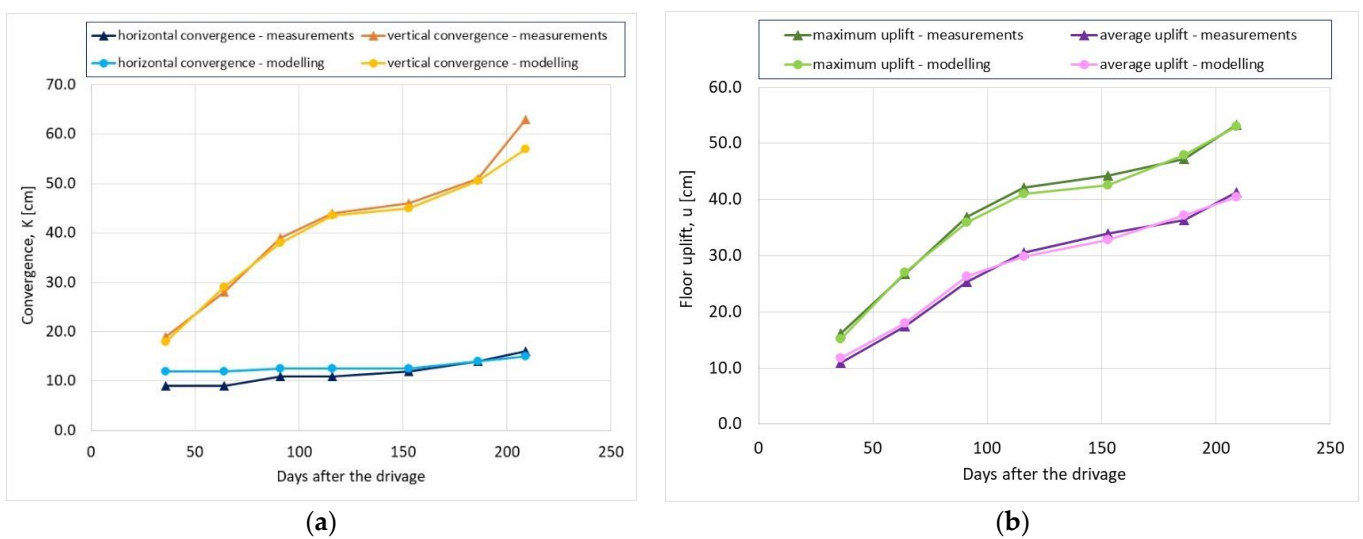


**Figure 16.** The consistency between numerical modeling and underground measurements of roadway F-33 deformation at chainage 405 m. (a) Convergence. (b) Floor uplift.

For the results of the numerical analysis, the  $m_b$  and  $s$  parameters of the Hoek–Brown criterion were reduced 209 days after the excavation, as follows:

- Claystone—a 43% decrease in the post-failure parameter  $m_b$  (at an approximate rate of 0.0016/day), and a 60% decrease in the parameter  $s$ .
- Mudstone—a 32% decrease in the post-failure parameter  $m_b$  (at an approximate rate of 0.0019/day), and a 43% decrease in the parameter  $s$ .
- Coal—an 8% decrease in the post-failure parameter  $m_b$  (at an approximate rate of 0.0007/day), and a 25% decrease in the parameter  $s$ .

The determined trendline functions of the post-failure parameters  $m_b$  and  $s$  are shown in Figures 17 and 18. The functions, as with roadway D-2, are exponential, and their determination coefficient  $R^2$  is in the range of 0.84–0.99.

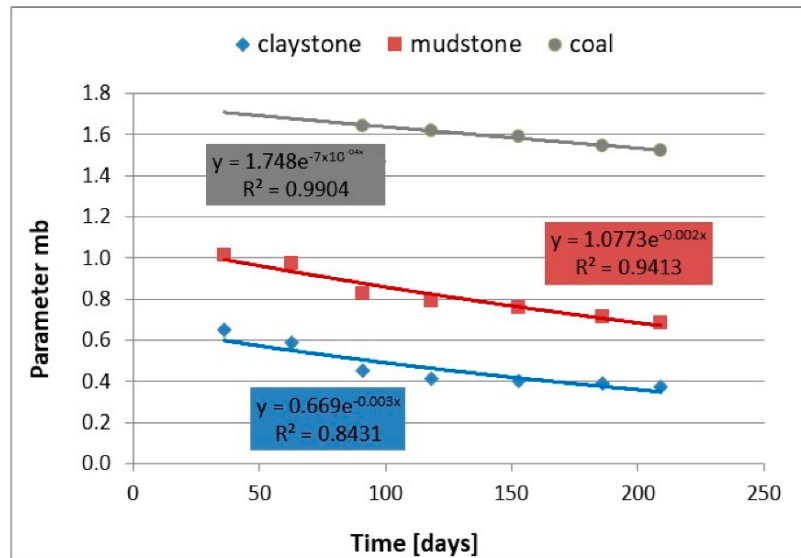


Figure 17. Changes in the post-failure parameter  $m_b$  of the rocks around roadway F-33—convergence-monitoring station at chainage 405 m.

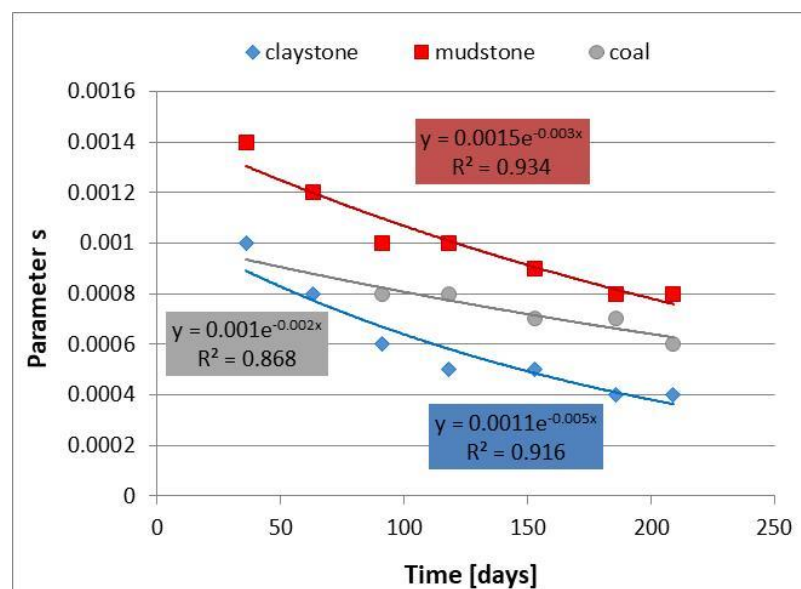
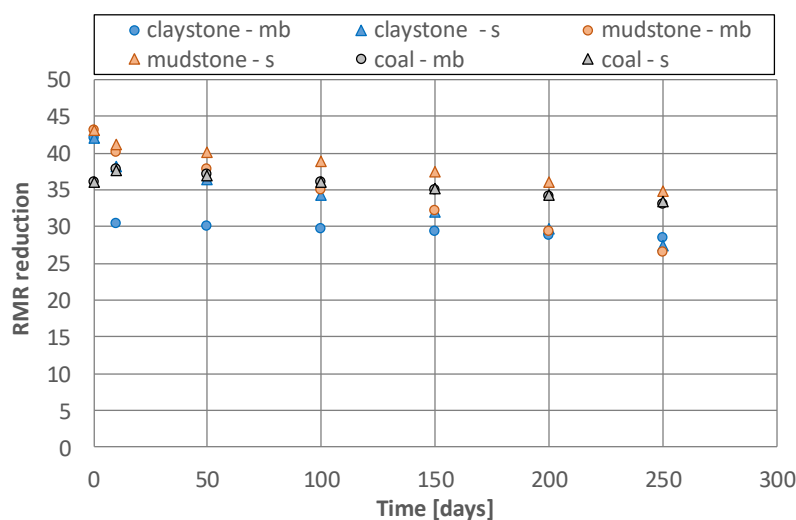


Figure 18. Changes in the post-failure parameter  $s$  of the rocks around roadway F-33—convergence-monitoring station at chainage 405 m.

The analysis of the RMR index reduction around roadway F-33 over 209 days showed that the best estimation was achieved for the change in the coal mass quality, which remained constant over the period considered (Figure 19). In the case of claystone, this

change increased up to 29%, and in the case of mudstone, it increased up to 31%, over the 209 days analyzed. In both cases, the cause of the calculated differences is an excessively rapid decrease in one of the analyzed parameters. The parameter  $s$  in the instance of claystone and the parameter  $m_b$  in the instance of mudstone indicate the need for a closer determination of the trend functions of the reduction in the empirical parameters of the Hoek–Brown criterion.



**Figure 19.** RMR decrease corresponding to  $m_b$  and  $s$  decrease versus time—rocks around roadway F-33.

### 3.4. Modeling of the Heave of Waterlogged Floor

As demonstrated earlier, the heave of the floor with underlying clay rocks is related to the reduction in their strength and deformability parameters. The reduction reflects the gradual process of rock-mass destruction and the slow filtration of water into the floor rocks. Therefore, the following procedure was established for the modeling of the waterlogged floor heave:

- First, the stress and deformation distribution for a set of geomechanical parameters of the rock mass was determined.
- The second step was the reduction in the strength and deformability parameters in the entire zone of destressed rock ( $\sigma_1 = 0$ ) beneath the floor in the model, where the reduction is in accord with the previously performed laboratory tests on the rock sample after 3 h of submerging in water.
- The third step was performing the subsequent numerical simulation and the reduction in the strength and deformability parameters for the expanded destressed zone, while, at the same time, reducing these parameters in the first zone to the values obtained from laboratory tests after 6 h of soaking with water.
- The fourth step was performing the third numerical simulation and the reduction in the strength and deformability parameters for the obtained expanded destressed zone, while simultaneously reducing these parameters for the first zone after 12 h of soaking, and for second zone after 6 h of soaking.
- The fifth step was performing the fourth simulation, and reducing the strength and deformability parameters for the obtained expanded zone, while simultaneously reducing these parameters for the first zone after 24 h of soaking, and for the second zone after 12 h of soaking, and for the third zone as if after 6 h of soaking.
- The sixth step was performing subsequent numerical simulations until the extent of the failure zone beneath the floor reaches the full width of the roadway.
- The seventh step was to continue performing numerical simulations until all the destressed rock beds beneath the floor are assigned geomechanical parameters as if after 24 h of soaking with water.

Therefore, prior to the modeling, the laboratory tests have to be carried out to establish the strength and deformability parameters of rocks from beneath the floor after 3, 6, 12, and 24 h of soaking with water. In the case of rock types other than clay rocks that change their properties with soaking relatively quickly, the duration of the rock soaking in the laboratory can be prolonged.

In order to determine the optimal time of the rock soaking to obtain the change in the mechanical and deformation rock parameters, it is best to carry out a preliminary swelling test and slaking test. The observations that determined the periods of soaking with water in the subsequent tests were: reaching approximately 80–90% of the final value of the swelling coefficient, or the cracking of the rock perpendicular to the stratification, and the breakdown of the rock into small pieces under the influence of water. In this study, the rock samples reached 80% of the final swelling coefficient within 22–28 h (Figure 20); therefore, the lengthiest period of soaking assumed for the subsequent rock tests was 24 h.

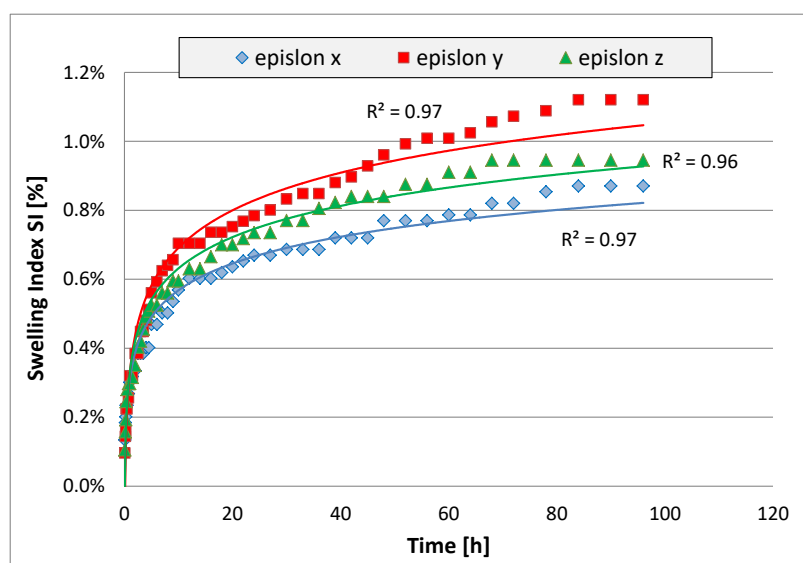


Figure 20. An example of results of swelling test on claystone from roadway F-33.

### 3.4.1. Roadway D-2

The numerical simulation for roadway D-2, following the previously described procedure, was performed in nine stages, in which the geomechanical parameters of the floor rocks were changed depending on the extent of the failure zone and water infiltration. The geomechanical parameters of the saturated rocks beneath the floor of roadway D-2 were obtained from laboratory tests before modeling. The changes in the specific weight, compressive strength, Poisson ratio, and Young modulus of the claystone were determined after 3, 6, 12, and 24 h of soaking with water (Figure 7). In this modeling procedure, the  $m_b$  and  $s$  parameters of the Hoek–Brown criterion for the floor rock were assumed to be constant, while the rock’s geomechanical parameters were subject to reduction (Table 5). For the remaining rocks around roadway D-2, the input geomechanical parameters were as shown in Table 1, and the Hoek–Brown criterion parameters are shown in Table 2.

Table 5. Geomechanical parameters of claystone from beneath the D-2 roadway floor, depending on time of exposure to water.

Time of Exposure to Water	$\gamma$ (kN)	$\nu$ (-)	$E$ (GPa)	$\sigma_c$ (MPa)	$m_b$	$s$
0 h	25.172	0.207	5.162	56.13		
3 h	25.295	0.252	4.844	50.57		
6 h	25.355	0.287	3.997	46.50	0.758	0.0007
12 h	25.441	0.309	3.484	42.65		
24 h	25.466	0.343	3.179	38.52		

The numerical analysis of the floor heave in roadway D-2 was based on the rock beds' position, as shown in Figure 4. The extent of the floor rocks' failure zone was determined at each model stage from the model-generated maps of the normal stress distribution.

The failure zone within the rocks beneath the floor was defined by the minimum and maximum principal stresses  $\sigma_1$  and  $\sigma_3$ , equal to 0 MPa. The subsequent enlarged failure zones were contoured until their extent reached the full width of the roadway.

In the first stage of the modeling, the input geomechanical parameters for the floor rocks were as obtained from the laboratory tests in dry conditions. The zone of the failure of the rocks with a maximum thickness of 65 cm was contoured based on the model-generated maps of the distribution of the stresses  $\sigma_1$  and  $\sigma_3$  around the roadway (Figure 21). The contours of the rock failure zone for the  $\sigma_1$  and  $\sigma_3$  stresses, respectively, are marked in red.

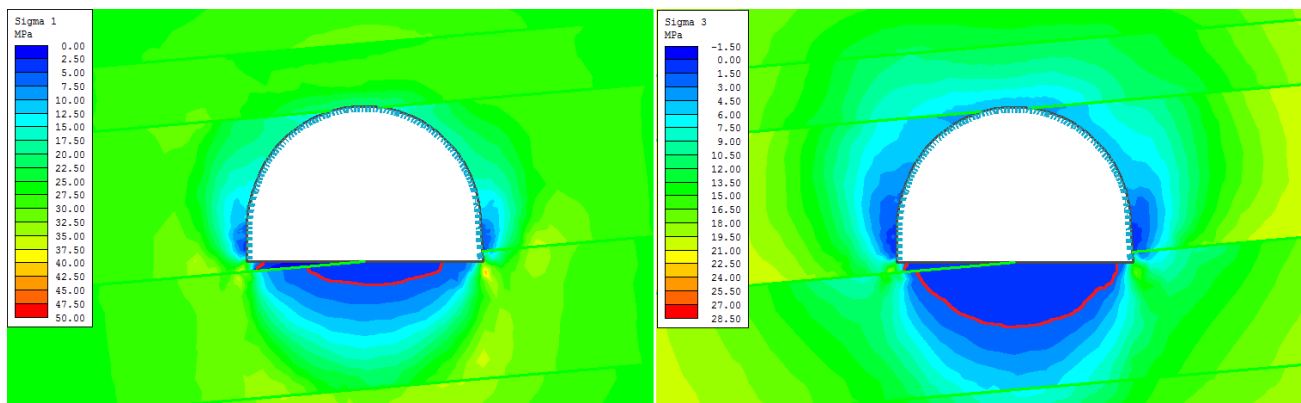


**Figure 21.** Extent of the failure zone beneath the dry floor of roadway D-2—stage 1.

In the second stage, the geomechanical parameters obtained from the laboratory tests on the rock samples after three hours of soaking (Table 5) were assigned to the failure zone contoured beneath the roadway floor. Next, the maps of the principal stresses were generated (Figure 22), and, again, the failure zone was contoured and enlarged up to 120 cm from the roadway floor.

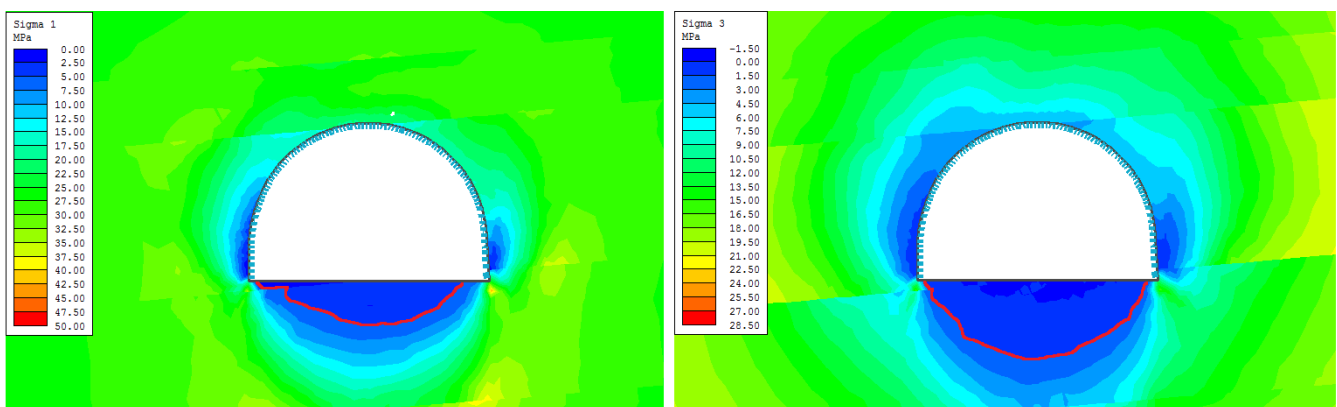


**Figure 22.** Extent of the failure zone beneath the waterlogged floor of roadway D-2—stage 2.

In the third stage, the geomechanical parameters within the previously delineated failure zones were further reduced. In this stage, these parameters for the first-stage failure zone were assumed to be as they were after six hours of soaking with water, whereas, for the second-stage failure zone, they were assumed to be as they were after three hours of soaking. Subsequently, the model produced the maps of the normal stress distributions and the failure zone, which reached 160 cm down from the roadway floor (Figure 23).

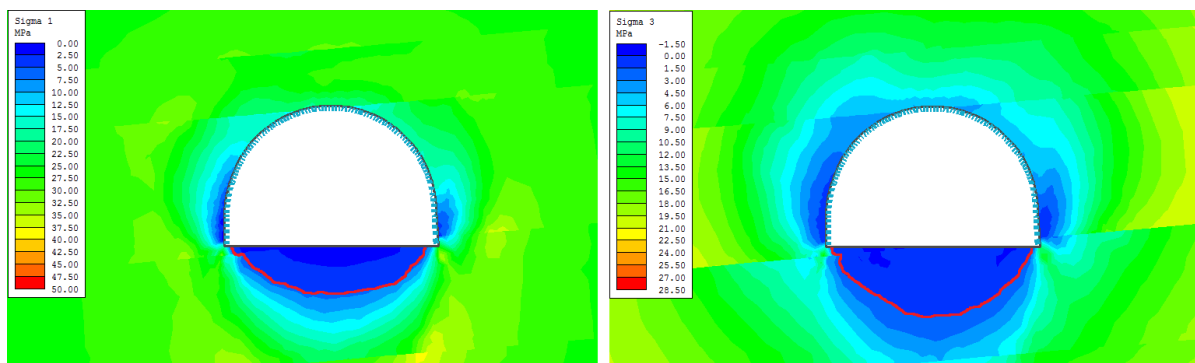


**Figure 23.** Extent of the failure zone beneath the waterlogged floor of roadway D-2—stage 3.

The fourth stage of the numerical modeling showed a further expansion of the failure zone down from the floor up to 185 cm (Figure 24). In this stage, the geomechanical parameters of the rocks within the failure zones of the earlier stages were set as if after 3 h of soaking for the third-stage zone, 6 h for the second-stage zone, and 12 h for the first-stage zone.

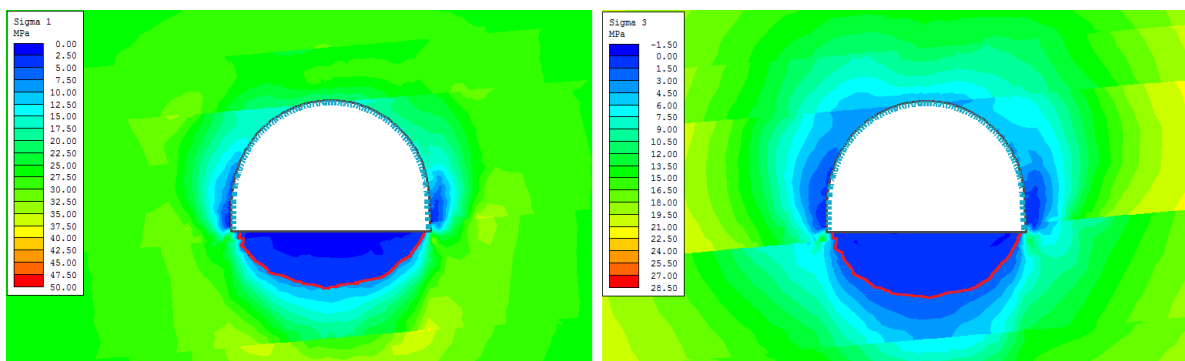


**Figure 24.** Extent of the failure zone beneath the waterlogged floor of roadway D-2—stage 4.

In the fifth stage, the failure zone expanded by 20 cm. Its geomechanical parameters were assumed, in accordance with the laboratory tests, to be as they were after three hours of soaking with water, whereas the parameters of the failure zones from the previous model stages were as they were after 6, 12, and 24 h soaking, respectively. In this stage, the horizontal extent of the failure zone beneath the floor reached the full width of the roadway (Figure 25). Therefore, in the following stages of the modeling, only the strength parameters of the rocks beneath the floor were changed until the whole weakened zone featured parameters as obtained after 24 h of soaking with water, at which point the modeling ended. Altogether, there were nine stages in the numerical modeling.

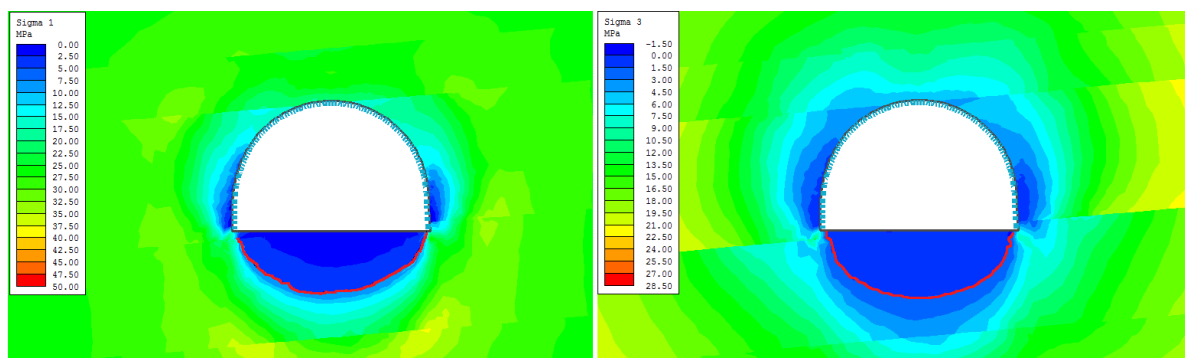


**Figure 25.** Extent of the failure zone beneath the waterlogged floor of roadway D-2—stage 5.

Figure 26 presents the propagation of the failure zone beneath the roadway floor at all stages of the numerical simulation. The gray color represents the geomechanical parameters of the floor rocks obtained from the tests on the samples under dry conditions. Green represents the rock of parameters after three hours of soaking with water, yellow represents the parameters after six hours, purple represents the parameters after 12 h, and blue represents the parameters after 24 h of soaking.

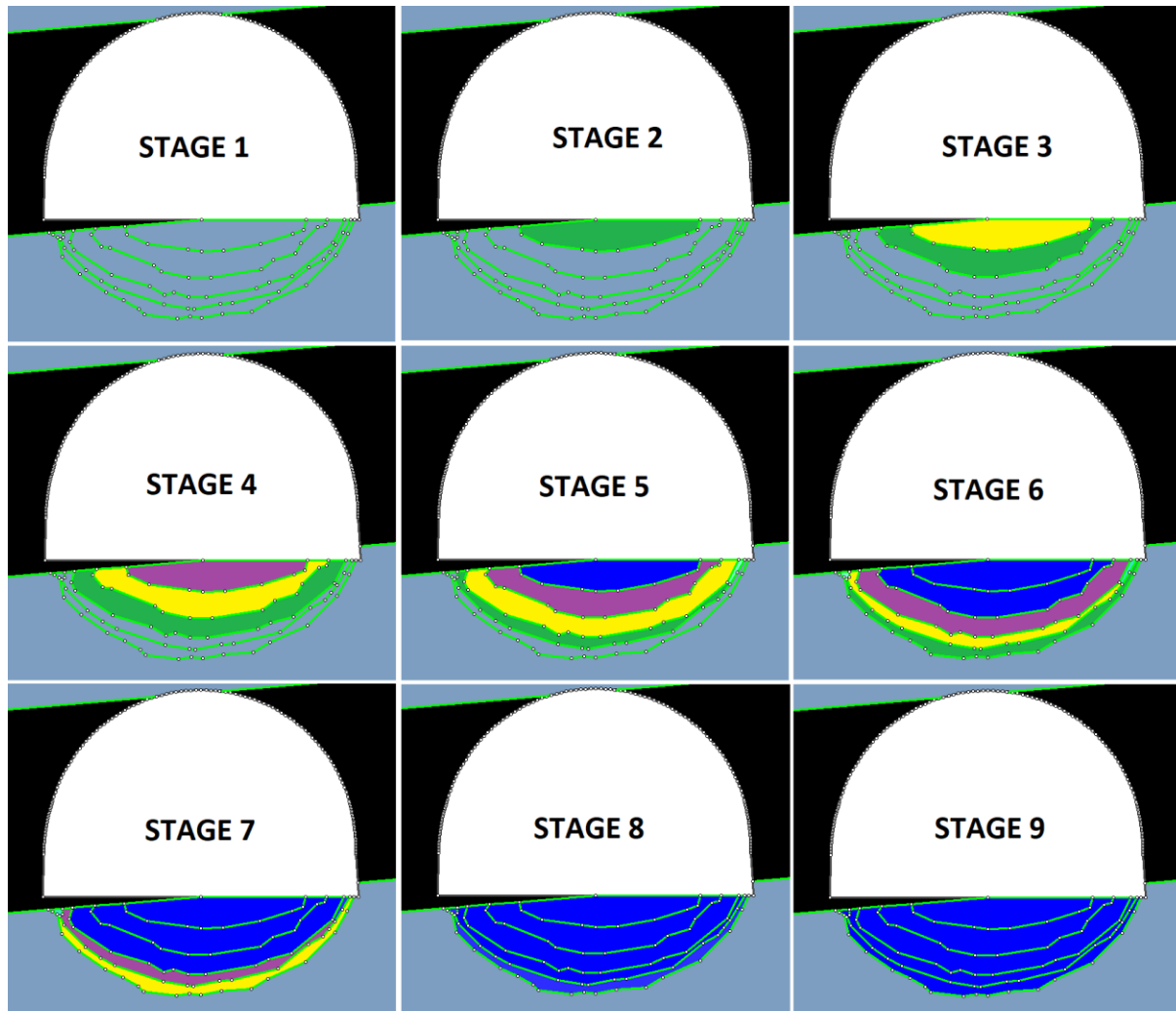


**Figure 26.** Stages of the numerical simulation of the impact of water saturation of the rocks beneath the floor of roadway D-2 on the magnitude of the floor heave, and with various geomechanical properties: gray color—dry rocks, green—rocks after 3 h of soaking with water, yellow—rocks after 6 h of soaking, purple—rocks after 12 h of soaking, dark blue—rocks after 24 h of soaking.

The performed numerical simulation generated a set of maps of the total deformation distribution around the excavation. These deformations are shown in Figure 27 and Table 6. The maximum floor heave obtained through the modeling was 1.20 m, the average floor heave was 0.92 m, the convergence of the sidewalls was 0.78 m, and the change in the roadway height was 1.14 m.

The results obtained from a series of simulations were compared with the in situ readings at the convergence station at the 614th meter of roadway D-2 [5]. The compilation of these data is presented in Table 6. It confirms that the results of the numerical simulation, based on the methodology described above, are highly consistent with the in situ measurements at the convergence station in the roadway. The concluding results of the average floor heave differ by 6.5%, and the maximum floor heave differs by 10.8%. It is

worth noting that in the condition of claystone beneath the floor weakened by water, the measured value of the floor heave constitutes 85% of the total vertical convergence (98 cm out of the overall value of 116.5 cm).

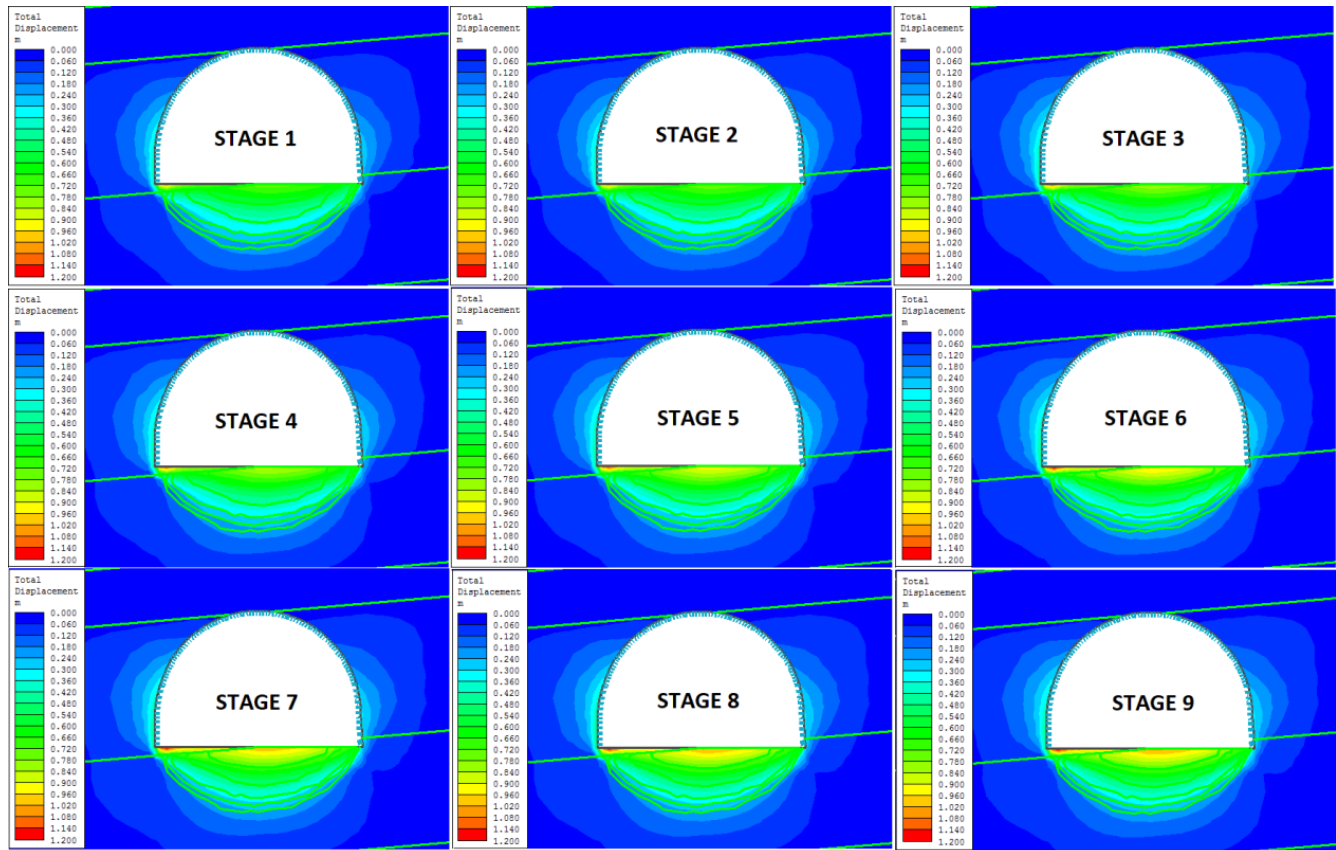


Figure 27. Convergence of the D-2 roadway versus the extent of the saturation zone in the floor rocks.

Table 6. Comparison of the convergence results from numerical model of roadway D-2 with the in situ measurements of the 614th meter of the roadway.

Research	Stage	$\Delta S$ (cm)	$u_{max}$ (cm)	$u_{av}$ (cm)	$\Delta H$ (cm)
numerical	I	72	102	65	84
	II	72	102	68	84
	III	72	108	71	90
	IV	72	108	73	96
	V	72	114	78	102
	VI	78	120	81	108
	VII	78	120	83	108
	VIII	78	120	88	108
	IX	78	120	92	114
in situ		79	107	98	116.5
difference (%)		1.3	10.8	6.5	2.2

### 3.4.2. Roadway F-33

There were ten stages in the numerical modeling of the floor heave in the waterlogged roadway F-33. In this case, as in the case of roadway D-2, the rocks beneath the floor were assigned different geomechanical parameters, depending on the extent of the failure zones and the degree of deterioration due to the saturation with water. The geomechanical parameters of the clay rocks from underneath the roadway floor (Figure 9) were determined through laboratory tests on samples of various degrees of saturation with water (Table 7).

**Table 7.** Geomechanical parameters of claystone from the floor of the roadway F-33 versus time of soaking with water.

Time of Exposure to Water	$\gamma$ (kN)	$\nu$ (-)	$E$ (GPa)	$\sigma_c$ (MPa)	$m_b$	$s$
0 h	30.552	59.64	5.575	0.200		
3 h	30.718	45.66	4.557	0.231		
6 h	30.849	40.96	4.144	0.273	0.681	0.0005
12 h	30.983	37.85	3.332	0.299		
24 h	31.126	33.73	3.095	0.316		

The rocks in other areas around roadway F-33 were assigned the geomechanical parameters presented earlier, in Table 3, and the parameters of the Hoek–Brown criterion, shown in Table 4.

The simulation sequence started from the dry conditions of the roadway floor and the rock mass parameters obtained from laboratory tests on the dry samples. The generated charts of the normal stress distributions around the roadway (Figure 28) were the basis for the failure zone range drawing of the maximum-thickness rock mass 95 cm below the floor. In the subsequent stages, the failure zone below the floor expanded, and its final depth from the roadway contour reached approximately 2 m. Figure 29 is an example of the distribution of the principal stresses  $\sigma_1$  and  $\sigma_3$  and the resulting failure zone after the fifth stage of the modeling, where the depth of the destructed and saturated rock mass reached around 1.55 m below the roadway floor.

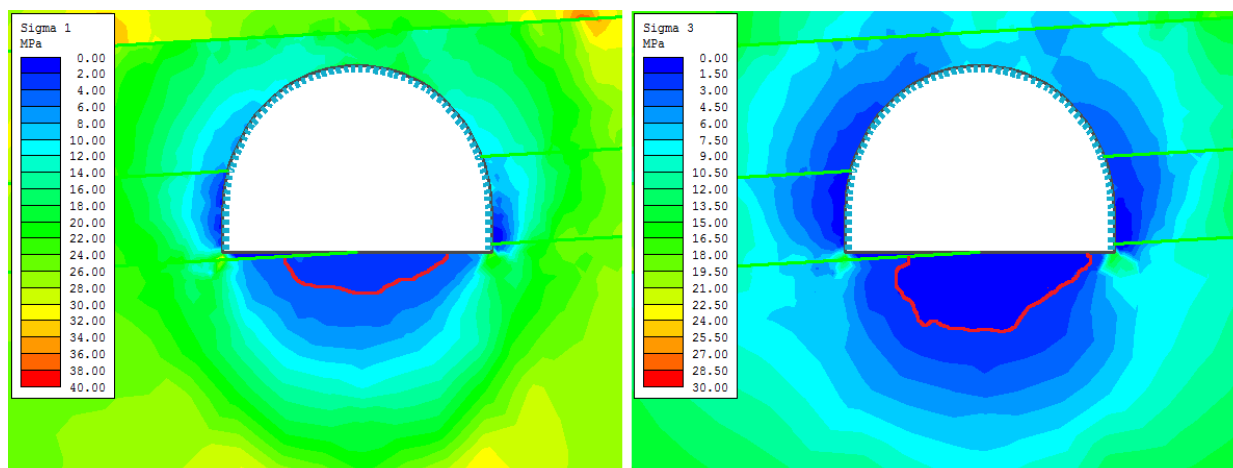


**Figure 28.** The extent of the failure zone in the floor of roadway F-33—stage 1.

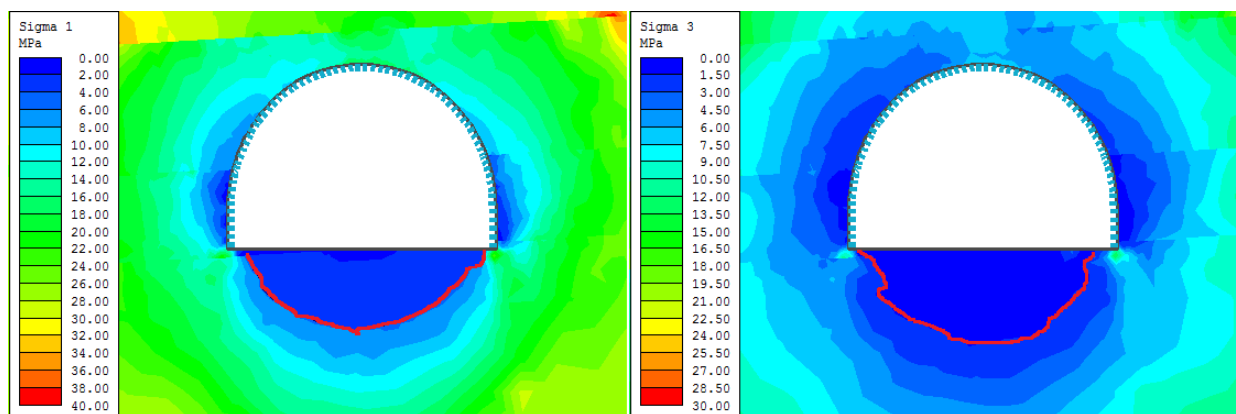


**Figure 29.** The extent of the failure zone beneath the floor of roadway F-33—stage 5.

Overall, the numerical simulation comprised 10 stages, which are shown on Figure 30. The figure illustrates the progress of the disintegration of the floor rocks and the water percolation into the rock mass. The same color scheme is used as that in Figure 23 i.e., the gray color represents the geomechanical parameters of the floor rocks obtained from the tests on the samples in dry conditions. Green represents the rock parameters after three hours of soaking with water, yellow represents the parameters after six hours, purple represents the parameters after 12 h, and blue represents the parameters after 24 h of soaking.

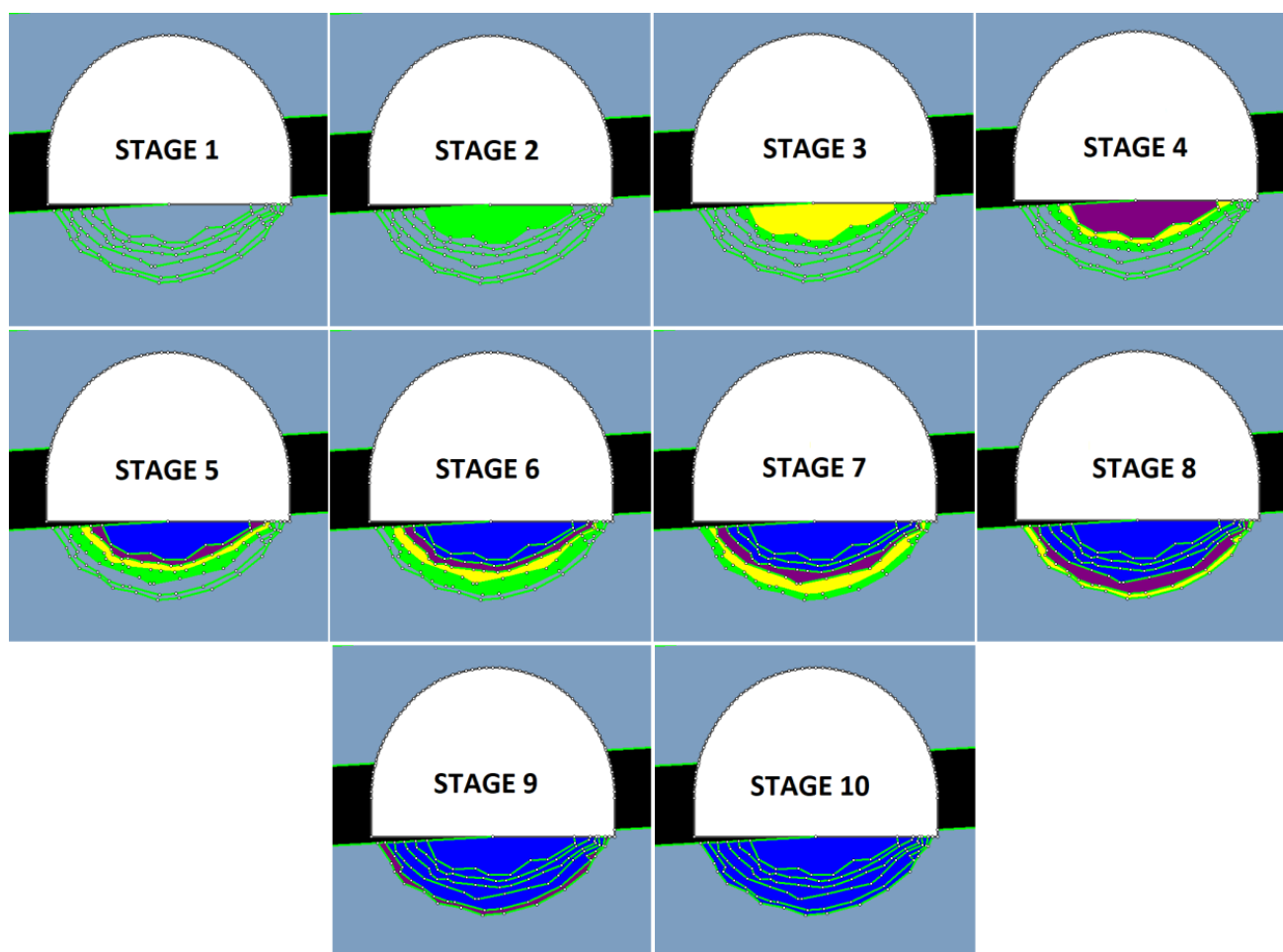


**Figure 30.** Stages of the numerical simulation of the impact of saturation of the rocks beneath the floor of roadway F-33 on the magnitude of the floor heave, and with various geomechanical properties: gray color—dry rocks, green—rocks after 3 h of soaking with water, yellow—rocks after 6 h of soaking, purple—rocks after 12 h of soaking, dark blue—rocks after 24 h of soaking.

A series of maps of the total deformation distribution around the excavation were generated through the numerical analysis. They are presented in Figure 31 and in Table 8. After the ten stages of the numerical simulation, the obtained maximum floor heave reached 0.90 m, the average floor heave was 0.66 m, the sidewalls' convergence was 0.36 m, and the height of the roadway section was reduced by 0.89 m. By reducing the input geomechanical parameters of the rocks along with the increasing saturation with water, the output average floor heave grew by 30%.

Once again, no significant influence was noted of the reduction in the geomechanical parameters of the floor rocks on the deformation of the roof of the excavation. The numerical simulation of the rock-mass deformation around roadway F-33 showed that the floor heave constituted 92–100% of the vertical convergence.

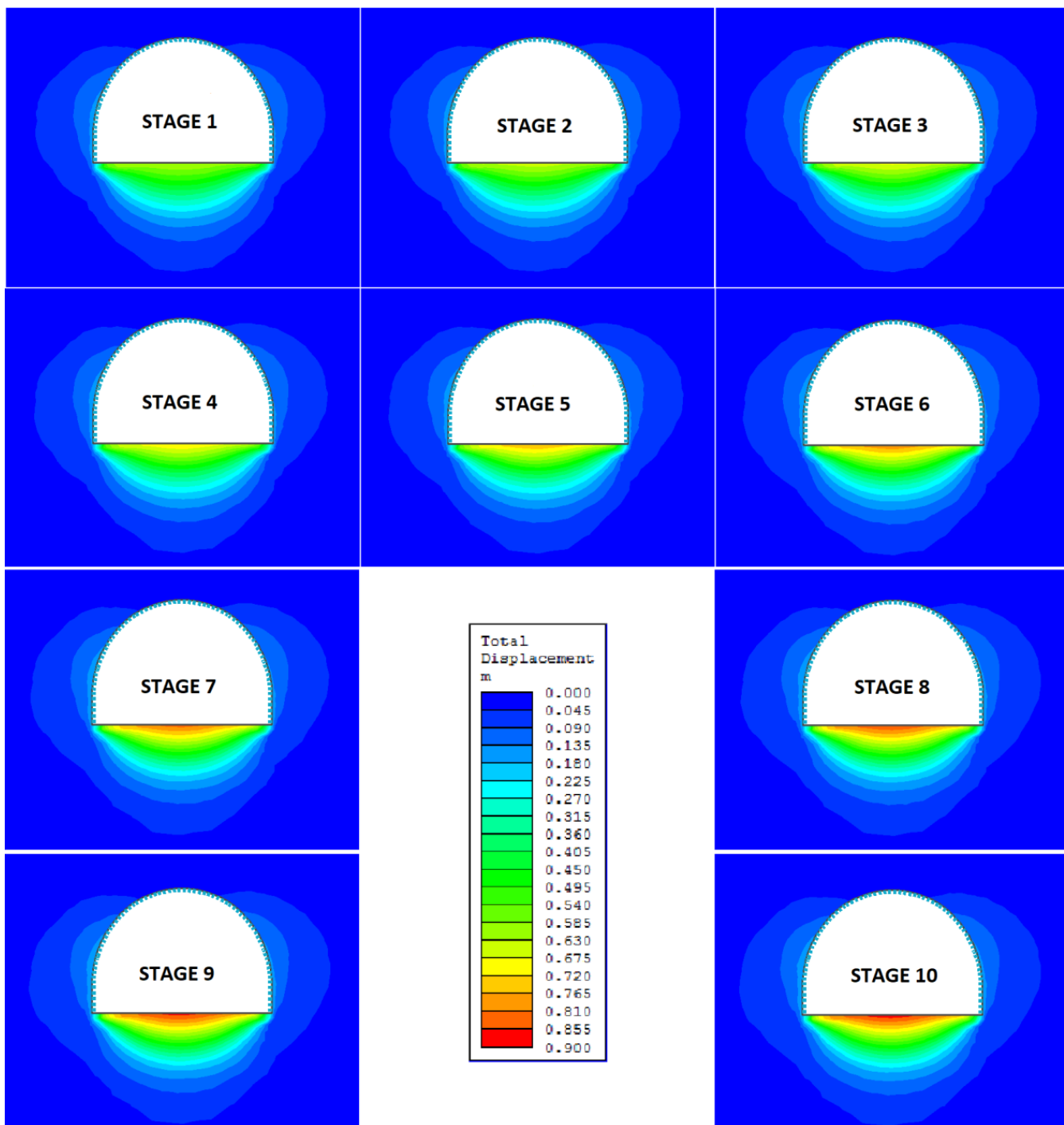


**Figure 31.** Convergence of roadway F-33 versus the extent of saturation zone in the floor rocks.

The in situ convergence measurements were carried out at the monitoring station at the 425th meter of roadway F-33. The maximum floor-heave reading by tape measure was 86 cm, and the average heave was 63 cm, 233 days after the roadway excavation. Moreover, the horizontal convergence of 38 cm and the vertical convergence of 90 cm almost entirely matched the results obtained from the numerical modeling (Table 8). The differences between the measured and simulated changes in the dimensions were 0% in the case of the height of the roadway, and 5.2% in the case of its width. Therefore, the method proved to be highly efficient.

**Table 8.** Comparison of the convergence results from numerical model of roadway F-33 with the in situ measurements on the 415th meter of the roadway.

Research	Stage	$\Delta S$ (cm)	$u_{max}$ (cm)	$u_{Av}$ (cm)	$\Delta H$ (cm)
numerical	1	31.5	63.0	50.8	67.5
	2	31.5	67.5	52.1	72.0
	3	31.5	67.5	53.4	72.0
	4	31.5	72.0	55.9	76.5
	5	31.5	76.5	57.2	81.0
	6	31.5	81.0	60.4	85.5
	7	31.5	85.5	63.6	90.0
	8	36.0	85.5	64.3	90.0
	9	36.0	85.5	65.5	90.0
	10	<b>36.0</b>	<b>90.0</b>	<b>65.8</b>	<b>90.0</b>
in situ		<b>38.0</b>	<b>86.0</b>	<b>63.0</b>	<b>90.0</b>
difference (%)		5.2	4.4	4.4	0

#### 4. Summary and Discussion

Two methods of modeling the floor heave in underground roadways were presented in this paper. These methods are applicable either to mining roadways or to tunnels, where floor-heaving problems are serious. Two common situations were considered:

- A roadway in a dry and non-soaking rock mass maintained for a long time;
- A waterlogged roadway with clay rocks beneath the floor.

Considering that the rocks around the roadways in coal mines are typically mudstones, or claystones, the second of the studied cases appears the most often, and the problem of the accurate evaluation of rock mass behavior is extensive. We are aware of the difficulties in the application of the presented modeling method.

This is because, in the first case, prior observations of the convergence in the adjacent roadway excavated in the same rocks is required, while the second case requires a series of laboratory tests to determine the mechanical properties of the floor rocks versus the saturation with water. Practice proves that collecting rock samples for laboratory testing, as stipulated for the second case, is much easier than obtaining convergence records, as is required for the first case. The convergence monitoring, for technological reasons, most often starts with a long delay, e.g., one or two months after the roadway excavation. In the tunnels, convergence monitoring usually starts immediately after the excavation and installation of the support. However, the convergence record needed for modeling purposes has to cover at least half a year.

In this paper, it is demonstrated that the high level of consistency between the modeling results and the in situ measurement and, at the same time, with the slightly different assessments of rock-mass quality in terms of RMR or GSI, can be achieved through a reduction in the H-B criterion parameters  $m_b$  and  $s$ . The time trend functions of the changes in both the Hoek–Brown empirical parameters have to determine similar changes in the RMR index. It seems that the differences in RMR evaluation over time in a range of 10–15% are acceptable from the perspective of mining practice. A further consideration should be the local variability in the RMR index along the roadway, which affects the initial parameters of the rock mass and their subsequent change.

In the case of the modeling of flooded floors, a series of laboratory tests of the strength and deformability of floor rocks must be carried out beforehand, where the duration of the soaking with water is a key factor. For this purpose, it is best to carry out a preliminary swelling test and slaking test to determine how long the swelling process lasts in a rock and after how much time laboratory tests on weakened rock should be carried out. This study shows that the rock should reach approximately 80–90% of the final value of the swelling coefficient, otherwise it will crack. Usually, the maximum swelling time is 24 h.

The consistency of the modeling and the observational results for the waterlogged roadway conditions is high. The differences are in a range of a few percent only, which

proves that the developed modeling methodology represents the actual behavior of the rock mass under the influence of water very accurately. As in our previous research, this paper indicates the need for the verification of the model by in situ measurements in underground excavations, which is the only way to prove its efficiency. The methodology presented in this article was tested on two roadways in two hard-coal mines.

The displacements of the waterlogged floor calculated by this method are particularly useful when estimating the magnitude of the support stress in the closed-support construction of roadways or the prediction of the maximum acceptable roadway floor uplift from the approved mining technology. The economic benefits achieved by early floor-uplift prediction should also be taken into account.

**Author Contributions:** Conceptualization, P.M. and Ł.O.; methodology, P.M. and Ł.O.; software, Ł.O.; underground research, Ł.O.; formal analysis, J.S.; resources, P.M. and J.S.; writing—original draft preparation, P.M.; writing—review and editing, P.M. and J.S.; visualization, P.M. and Ł.O.; supervision, P.M. All authors have read and agreed to the published version of the manuscript.

**Funding:** This research received no external funding.

**Institutional Review Board Statement:** Not applicable.

**Informed Consent Statement:** Not applicable.

**Data Availability Statement:** Not applicable.

**Conflicts of Interest:** The authors declare no conflict of interest.

## References

- Guo, G.; Kang, H.; Qian, D.; Gao, F.; Wang, Y. Mechanism for Controlling Floor Heave of Mining Roadways Using Reinforcing Roof and Sidewalls in Underground Coal Mine. *Sustainability* **2018**, *10*, 1413. [\[CrossRef\]](#)
- Xu, Y.; Chen, J.; Bai, J. Control of floor heaves with steel pile in gob-side entry retaining. *Int. J. Min. Sci. Technol.* **2016**, *26*, 527–534. [\[CrossRef\]](#)
- Liu, S.; Bai, J.; Wang, X.; Wu, B.; Wu, W. Mechanisms of Floor Heave in Roadways Adjacent to a Goaf Caused by the Fracturing of a Competent Roof and Controlling Technology. *Shock Vib.* **2020**, 5632943. [\[CrossRef\]](#)
- Lai, X.; Xu, H.; Shan, P.; Kang, Y. Research on Mechanism and Control of Floor Heave of Mining-Influenced Roadway in Top Coal Caving Working Face. *Energies* **2020**, *13*, 381. [\[CrossRef\]](#)
- Malkowski, P.; Ostrowski, L.; Bednarek, L. The Effect of Selected Factors on Floor Upheaval in Roadways—In Situ Testing. *Energies* **2020**, *13*, 5686. [\[CrossRef\]](#)
- Kang, Y.; Liu, Q.; Gong, G.; Wang, H. Application of a combined support system to the weak floor reinforcement in deep underground coal mine. *Int. J. Rock Mech. Min. Sci.* **2014**, *71*, 143–150. [\[CrossRef\]](#)
- Gong, P.; Ma, Z.; Ni, X.; Zhang, R.R. Floor heave mechanism of gob-side entry retaining with fully-mechanized backfilling mining. *Energies* **2017**, *10*, 2085. [\[CrossRef\]](#)
- Wang, P.; Jiang, L.; Ma, C.; Yuan, A. Evolution Laws of Floor Stress and Stability of Floor Roadway Affected by Overhead Mining. *Earth Sci. Res. J.* **2021**, *24*, 45–54. [\[CrossRef\]](#)
- Li, C.; Zuo, J.; Chunchan, W.; Xu, X. Fracture Development at Laminated Floor Layers Under Longwall Face in Deep Coal Mining. *Nat. Resour. Res.* **2020**, *29*, 3857–3871. [\[CrossRef\]](#)
- Sun, X.; Wang, D.; Feng, J.; Zhang, C.; Chun, Y. Deformation control of asymmetric floor heave in a deep rock roadway: A case study. *Int. J. Min. Sci. Technol.* **2014**, *24*, 799–804. [\[CrossRef\]](#)
- Feng, Q.; Jiang, B. Analytical solution for stress and deformation of the mining floor based on integral transform. *Int. J. Min. Sci. Technol.* **2015**, *25*, 581–586. [\[CrossRef\]](#)
- Jun-jie, H.; Ya-guang, Q.; Shuang, Z.; Wei, W.; Lei, W. Strength response characteristics and coupling support of deep roadway in soft rock masses. *Cogent Eng.* **2017**, *4*, 1339337. [\[CrossRef\]](#)
- Walentek, A. Analysis of the Applicability of the Convergence Control Method for Gateroad Design Based on Conducted Underground Investigations. *Arch. Min. Sci.* **2019**, *64*, 765–783.
- Mo, S. Floor Heave Mechanisms in Underground Coal Mine Roadways. Ph.D. Thesis, Faculty of Engineering, UNSW, Sydney, Australia, 2019.
- Feng, G.; Li, S.; Wang, P.; Guo, J.; Qian, R.; Sun, Q.; Hao, C.; Wen, X.; Liu, J. Study on Floor Mechanical Failure Characteristics and Stress Evolution in Double Pre-driven Recovery Rooms. *Math. Probl. Eng.* **2020**, 9391309. [\[CrossRef\]](#)
- Yu, X.; Liu, Y.; Fan, H. Research on Destroyed Floor Depth—The Example of the 51302 Working Face in the Liangzhuang Coal. *Res. Sq.* **2021**. [\[CrossRef\]](#)

17. Zhai, J.; Liu, D.; Li, G.; Wang, F. Floor Failure Evolution Mechanism for a Fully Mechanized Longwall Mining Face above a Confined Aquifer. *Adv. Civ. Eng.* **2019**, 8036928. [[CrossRef](#)]
18. Jin, S.; Lianguo, W. Numerical simulation of grooving method for floor heave control in soft rock roadway. *Min. Sci. Technol.* **2011**, *21*, 49–56. [[CrossRef](#)]
19. Kyle, P.; Joel, B.; Kot, U.; Mark, K. Mitigation of floor heave in West Kentucky Coal Mine. *Int. J. Min. Sci. Technol.* **2016**, *26*, 521–525. [[CrossRef](#)]
20. Guo, Z.; Du, Z.; Hu, S.; Zhang, X.; Wang, K.; Guo, J. Comprehensive Treatment Methods of Floor Heave Disasters in Mining Areas of China. *Geotech. Geol. Eng.* **2017**, *35*, 2485–2495. [[CrossRef](#)]
21. Shi, L.; Zhang, H.; Wang, P. Research on Key Technologies of Floor Heave Control in Soft Rock Roadway. *Adv. Civ. Eng.* **2020**, 8857873. [[CrossRef](#)]
22. Guo, B.H.; Lu, T.K. Floor Heave Behavior and Control of Roadway Intersection in Deep Mine. In *Geotechnical Aspects of underground Construction in Soft Ground, Proceedings of the 6th International Symposium Shanghai 2008, Shanghai, China, 10–12 April 2008*; Ng, C.W.W., Huang, H.W., Liu, G.B., Eds.; CRC Press: London, UK, 2008. [[CrossRef](#)]
23. Aghababaei, S.; Saeedi, G.; Jalalifar, H. Risk Analysis and Prediction of Floor Failure Mechanisms at Longwall Face in Parvadeh-I Coal Mine using Rock Engineering System (RES). *Rock Mech. Rock Eng.* **2016**, *49*, 1889–1901. [[CrossRef](#)]
24. Liu, W.; Mu, D.; Xie, X.; Yang, L.; Wang, D. Sensitivity Analysis of the Main Factors Controlling Floor Failure Depth and a Risk Evaluation of Floor Water Inrush for an Inclined Coal Seam. *Mine Water Environ.* **2018**, *37*, 636–648. [[CrossRef](#)]
25. Mo, S.; Ramandi, H.L.; Oh, J.; Masoumi, H.; Canbulat, I.; Hebblewhite, B.; Saydam, S. A new coal mine floor rating system and its application to assess the potential of floor heave. *Int. J. Rock Mech. Min. Sci.* **2020**, *128*, 104241. [[CrossRef](#)]
26. Pimentel, E. Existing methods for swelling tests—A critical review. *Energy Procedia* **2015**, *76*, 96–105. [[CrossRef](#)]
27. Malkowski, P.; Ostrowski, L.; Bozecki, P. The impact of the mineral composition of Carboniferous claystones on the water-induced changes of their geomechanical properties. *Geol. Geophys. Environ.* **2017**, *43*, 43–55. [[CrossRef](#)]
28. Tang, S.B.; Tang, C.A. Numerical studies on tunnel floor heave in swelling ground under humid conditions. *Int. J. Rock Mech. Min. Sci.* **2012**, *55*, 139–150. [[CrossRef](#)]
29. Erguler, Z.A.; Ulusay, R. Water-induced variations in mechanical properties of clay-bearing rocks. *Int. J. Rock Mech. Min. Sci.* **2009**, *46*, 355–370. [[CrossRef](#)]
30. Hoek, E. Practical Rock Engineering. Hoeks' Corner. 2007. Available online: <https://www.rocsience.com/learning/hoeks-corner> (accessed on 24 January 2022).
31. Bieniawski, Z.T. *Engineering Rock Mass Classifications*; Wiley: New York, NY, USA, 1989.
32. Davarpanah, S.M.; Ván, P.; Vásárhelyi, B. Investigation of the relationship between dynamic and static deformation moduli of rocks. *Geomech. Geophys. Geoenergy Georesour.* **2020**, *6*, 29. [[CrossRef](#)]
33. Malkowski, P.; Ostrowski, L. Convergence monitoring as a basis for numerical analysis of changes of rock-mass quality and Hoek-Brown failure criterion parameters due to longwall excavation. *Arch. Min. Sci.* **2019**, *64*, 93–118. [[CrossRef](#)]
34. Wei, X.; Zuo, J.; Shi, Y.; Liu, H.; Jiang, Y.; Liu, C. Experimental verification of parameter m in Hoek-Brown failure criterion considering the effects of natural fractures. *J. Rock Mech. Geotech. Eng.* **2020**, *12*, 1036–1045. [[CrossRef](#)]